ELECTROMECHANICAL BEHAVIOR OF PZT THIN FILM COMPOSITES FOR RF-MEMS

BY

SIVAKUMAR NAGA YAGNAMURTHY

THESIS

Submitted in partial fulfillment of the requirements
for the degree of Master of Science in Aerospace Engineering
in the Graduate College of the
University of Illinois at Urbana-Champaign, 2009

Urbana, Illinois

Advisor:

Associate Professor Ioannis Chasiotis, Director of Research

ABSTRACT

The mechanical and piezoelectric behavior of freestanding Lead Zirconate Titanate (PZT) composite films comprised of SiO_2, Pt, PZT and Pt, for MEMS applications was investigated by microscale uniaxial tension experiments. Due to the difficulty in fabricating individual freestanding PZT films, thin film stacks were fabricated in combinations of Silicon Oxide (SiO_2), Titanium (Ti), Platinum (Pt) and PZT. The specimens tested were stacks of SiO_2-TiPt-PZT-Pt, SiO_2-TiPt-PZT, SiO_2-TiPt, and individual SiO_2 and Pt thin films, with gauge lengths of 1,000 μm and widths of 50-100 μm. Full-field strain measurements were conducted with the aid of a fine speckle pattern (1 μm particle size) generated on the samples and the elastic modulus and Poisson's ratio were calculated by means of digital image correlation. The composite mechanical properties of the PZT stacks were computed from the stress vs. strain plots, while the mechanical properties of individual PZT films were extracted from those of the PZT stacks and the properties of SiO_2 and Pt films. It was found that the mechanical response of the PZT layer is non-linear but non-hysteretic, deviating from linearity at 0.35%. Failure is initiated in the PZT layer while the Pt films delay fracture, especially in SiO_2-TiPt-PZT-Pt stacks.

In addition to the elastic and failure mechanical properties of PZT, the d_{31} piezoelectric coefficient and the effect of applied stress on the magnitude of the hysteresis curves were investigated. The d_{31} coefficient was measured from the out-of-plane deflection of biased PZT specimens with dimensions similar to those tested previously. An analytical solution for the bending of a multilayered piezoelectric beam was used to compute d_{31} as 385±45 pm/V. An alternating field induced in-plane stress hysteresis loops which were asymmetric at small applied pre-stress, then becoming of equal magnitude as the pre-stress increased to hundreds of MPa. Similarly, the intersection of the hysteresis loops shifted from negative to positive electric field at stresses larger than 150 MPa. The applied pre-stress resulted in reduction of the hysteresis in the field induced in-plane stress loops, due to mechanical constraints imposed on 90° domain switching.

ACKNOWLEDGMENTS

I am grateful to my advisor Prof. Ioannis Chasiotis for giving me a great opportunity to work on this project together with his constant support and invaluable guidance during the course of this research. I would also like to acknowledge the Army Research Office Grant #W911NF0510063 and the National Science Foundation Grant #0555787 for providing financial support to carry out this research. I would also like to thank Dr. Ronald Polcawich from the Army Research Lab for providing specimens required for the research study. I also like to express thanks to Prof. John Lambros for providing relevant valuable discussions and for allowing the use of his lab instruments. Additionally, thanks to the staff of the Aerospace Engineering Department for their help in many occasions concerning administrative issues.

I would also like to thank my former colleague and mentor, Dr. Krishna Jonnalagadda, for comprehensively teaching me the experimental techniques required for this study. I enjoyed all the insightful discussions with my present and past colleagues Tanil, Nikhil, Salman, Pavan, David, Mohammad, and Qi in NanoMechanics Research Lab and would like to thank them for their support and companionship throughout the research. I also acknowledge the MRL staff members, Vania Petrova and Jim Masson for the training and timely assistance on the usage of SEM instruments. Finally, I am grateful for my family, friends and relatives for their extended love and support throughout my life.

TABLE OF CONTENTS

CHAPTER 1

INTRODUCTION

Advancements in surface microfabrication of materials have led to microelectromechanical systems (MEMS) that are small, compact and can perform the tasks of larger scale machines. These devices are commonly fabricated on a silicon substrate as thin film structures deposited in a sequence of individual layers, followed by selective etching to obtain the desired and often intricate shapes. Manufacturing processes include chemical vapor deposition, sputtering, chemical solution deposition and electro-deposition. Patterning is carried out by masking selected regions with a layer of a photoresist in order to etch redundant materials by wet or dry chemical processes. Characteristic examples of MEMS fabricated by the aforementioned processes are shown in Figure 1.1: A top view of a surface micro-machined gear assembly is shown in Figure 1.1(a), while a thin film capacitance-based microphone comprised of polysilicon plates is shown in Figure 1.1(b).

MEMS devices have been used as sensors because of their small size and the ability to integrate with microelectronics. They have been used quite widely as air bag pressure sensors in automobiles [1], nozzles in inkjet printers [2], accelerometers in gaming devices [3], micromirrors in LCD projectors [4] and interferometric modulator displays for mobile phones [5]. During use, they are often subjected to complex stress and strain states, due to which, their degrading mechanical response can adversely affect the performance of the overall application. Therefore, although conceptual designs of complex MEMS devices for various applications have been developed, the mechanical reliability and durability issues associated with these devices have made them far from reality. Since MEMS structures are very thin, minor defects, such as voids or cracks, can

lead to catastrophic failure although packaging methods have been developed to mitigate the effect of impact loads [6]. Hence, it is important to quantify the mechanical behavior of the thin film structural materials incorporated in MEMS in order to design devices that are less prone to mechanical failure with greater performance accuracy and reliability.

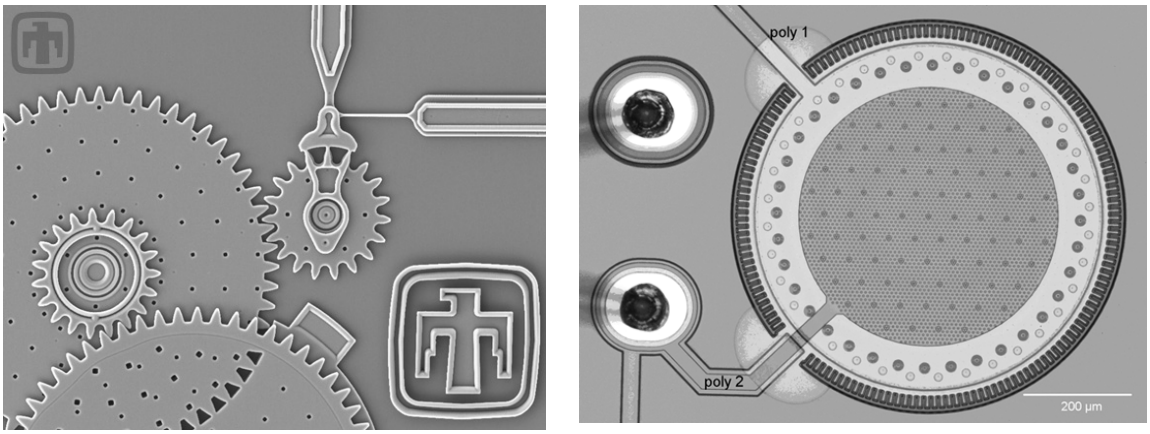

(a) **(b)**

Figure 1.1 (a) MEMS transmission gears [7]. **(b)** MEMS microphone containing polysilicon plates acting as capacitors [8].

1.1 Thin Film PZT Structures

In the recent years Lead Zirconium Titanate (PZT) has emerged as a new multifunctional material for MEMS, which has piezoelectric properties and has purely brittle mechanical behavior. PZT changes shape upon the application of an electric field, and similarly, an applied stress results in net electric charge on its surface. The physics behind the piezoelectric behavior is discussed in Chapter 3. Utilizing these phenomena, MEMS devices based on PZT thin films, such as RF switches [9], microphones, microscale robots and flapping wing micro-aerial vehicles [10,11], have been conceptualized but very few of them have been successful due to limitations arising from their mechanical reliability. As an example, a PZT MEMS switch [12] is shown in Figure

1.2, which is composed of a multimorph with a Au contact cantilever bonded on the top and a Au circuit micromachined on silicon substrate. The PZT multimorph, composed of SiO_2, Pt, PZT and Pt layers, bends out-of-plane upon biasing the Pt electrodes and, as a result, the Au contact cantilever closes the circuit. These films generate high actuation forces upon application of an electric potential and vice versa, which makes them useful as high precision microactuators, accelerometers, pressure sensors, energy harvesters (backpack straps, shoes etc), etc. [13-18].

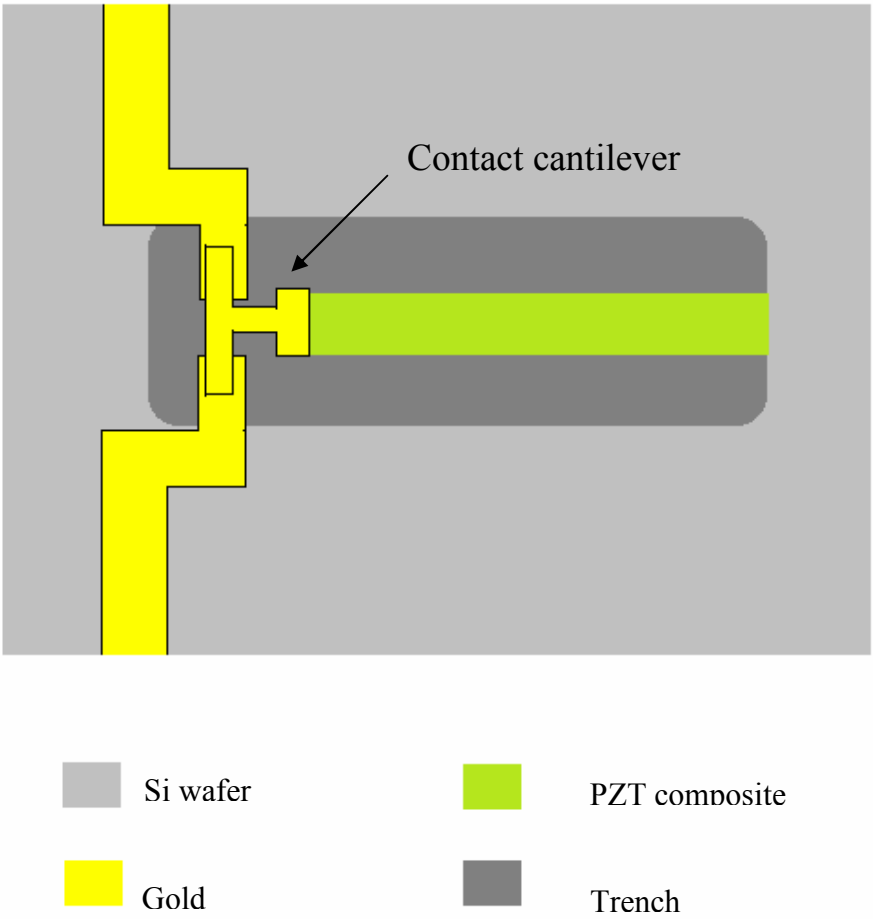

Figure 1.2 PZT MEMS switch in closed configuration. Redrawn from reference [12].

Piezoelectric actuation can be better than conventional thermal and electrostatic comb-driven actuation in MEMS devices involving moving components, as it eliminates the problems of Joule heating and the lateral instability of the comb-teeth [19-22]. However, due to limited data on the material properties of PZT thin films, better understanding of the piezomechanical behavior of PZT thin film structures is required to ensure their mechanical performance and reliability. This has to be put in perspective of the rather complex structure of PZT-based MEMS: due to their ceramic-like nature, PZT thin films are polarized through firmly bonded electrodes, such as Au, Pt, which are of thicknesses that are at most one order of magnitude thinner than the actual PZT films. Silicon dioxide is also deposited to make them electrically and thermally insulating. The mechanical and failure properties of each of these films are a function of their fabrication conditions and, therefore, experimental knowledge of the mechanical behavior of the individual layer materials is needed to predict the piezomechanical performance and reliability of the entire PZT stack.

Over the last decade, there have been several studies to understand mechanical behavior of thin films made for MEMS, such as Au and polysilicon, as a function of their grain size [23-25], porosity [26], texture [27], film thickness [28,29], strain rate [30,31] and manufacturing conditions [32]. However, the current literature on PZT film mechanics is limited, and the elastic modulus and strength values show large variations. Bhar *et al* [33] investigated the hardness, elastic modulus and fracture behavior of solution prepared PZT thin films by nanoindentation. Their PZT thin films exhibited harnesses between 5-8 GPa, which is lower than that for bulk PZT (9 GPa). Their indentation experiments caused fracture that remained at the sub-surface without creating delamination. However, it has also been reported that conventional indentation does not yield accurate modulus values due to the non-linear behavior of PZT thin films. Fang *et al* [34] investigated the effect of annealing temperature, also by nanoindentation, on the mechanical properties of PZT thin films. They reported a reduction in surface roughness and an increase in the modulus and hardness as the annealing temperature increased. The Young's modulus and hardness ranged from 110 – 260 GPa and 6.49 - 16.63 GPa, respectively, for annealing temperatures 600°C, 700°C, and 800°C. Zhou *et al* [35] used membrane deflection experiments to measure the properties of PZT composite films

including layers of SiO_2-TiPt. Their average values for the Young's modulus was 119 GPa. In another study, bulge tests by Hong *et al* [36] provided the elastic modulus of PZT films used in piezoelectric ink jet heads. Their multilayered specimens subjected to bulge test were made of a stack of polysilicon, SiO_2, Pt, PZT and Pt. Pressurized air was applied and full-field optical imaging was used to measure the deflection of the films in order to obtain the Young's modulus of PZT and polysilicon. They reported modulus values of 110 GPa and 49 GPa for polysilicon and PZT, respectively, both of which are lower than previous reports and theoretical values. The 30-50% lag in the modulus of polysilicon was attributed by the authors to defects such as microvoids and cracks at grain boundaries between columnar grains. In another study by Wakabayashi *et al* [37], the Young's modulus of PZT was measured as a function of annealing time and temperature. Membrane bending was used to test RF magnetron sputtered PZT membranes over a fine layer of platinum deposited on a silicon wafer. The study reported an increase in the Young's modulus of PZT with increased annealing temperature and time. When compared to the modulus of 22.7 GPa for as deposited specimens, annealed specimens at 700°C had an improved modulus of 76.6 GPa with higher built-in stresses. The authors attributed this increase in the modulus to film structure transformation and to Lead (Pb) loss during annealing. To date, all studies have measured the mechanical properties of PZT thin films mainly by nanoindentation and membrane bending and the reported moduli range from 40 – 127 GPa.

An important layer in the PZT stacks is SiO_2 which has many other uses as inter-level and gate dielectric in metal-oxide-semiconductor field effect transistors (MOSFETs) [38] and thin film transistors (TFTs) [39], in protective layers in metallic mirrors [40] and in anti-reflection coatings [41]. In the present work, thin SiO_2 and Pt layers were firmly bonded to PZT and therefore, their quantified mechanical behavior was also important. SiO_2 is used in PZT multimorphs as a thermal and electrical insulating layer, while Pt serves as electrode to bias the PZT. Over the last two decades, SiO_2 thin films have been investigated for their properties by nanoindentation [42], bulge tests [43], resonance tests [44] and uniaxial tensile tests [45,46]. Helvaci et al [42] used nanoindentation to investigate the mechanical properties of thermally grown SiO_2 on a silicon wafer. The substrate effect was isolated by using Saha and Nix's models to

deduce the "film only" properties: a modulus of 88 GPa was reported and was independent of the film thickness. Bulge tests were employed by Yang *et al* [43] to measure the mechanical properties of SiO_2 and Si_3N_4 thin films. Differential pressure was applied on SiO_2-SiN_x membrane specimens and load-deflection measurements were used along with a comprehensive mechanical model to calculate a modulus of 69.8 GPa with failure strength of 800 MPa. Su *et al* [44] used a similar membrane bending technique but the load was applied by a micro-probe on the SiO_2-SiN_x bilayer. The mechanical properties of individual layers were extracted from theoretical models. The modulus for low temperature SiO_2 thin films was reported as 41 GPa, which is significantly lower than expected. Sharpe *et al* [45] and Lin *et al* [46], used microscale tensile testing to measure moduli of 60.1±3.4 GPa and 65±3 GPa, respectively, while a fracture strength of 364±57 MPa was reported by Sharpe *et al*. Researchers also reported a modulus of 56.69±0.24 GPa for 1 μm thick SiO_2 by using a resonance technique.

From the aforementioned discussion, it becomes apparent that the mechanical properties of thin film PZT and SiO_2 reported by various studies in the literature differ significantly. While these differences can be attributed to fabrication and physical differences, such as film thickness, grain size, porosity and defects, the experimental techniques are also a serious cause for the scatter in the mechanical properties. Nanoindentation studies have the fundamental limitation of measuring the mechanical behavior of the entire composite structure and are the least useful in providing the ultimate strain and the material Poisson's ratio. Uniaxial tensile testing is more reliable compared to other methods and provides all mechanical properties, such as the Young's modulus, fracture strength, failure strain and the Poisson's ratio, but not the material hardness. Hence, one of this dissertation's goals was to employ microscale uniaxial tension experiments along with full field strain measurements to evaluate the mechanical properties of composite films made of PZT, Pt and SiO_2.

In addition to the mechanical behavior of the PZT stacks, appropriate design of PZT MEMS devices also requires knowledge of the piezoelectric behavior of PZT, which depends on the fabrication method, the residual stresses, the poling state and the microstructure of PZT. Very scarce data exist in literature on this topic and their

applicability to the present PZT stacks is very doubtful. Therefore, the second objective of this dissertation research was to quantify experimental the piezoelectric behavior of the PZT thin films at hand and, specifically, the piezoelectric coefficient d_{31}. Chapter 3 provides a detailed account of the existing literature values for the piezoelectric coefficients of thin PZT films and the effect of residual stresses on the hysteretic response of PZT.

1.2 Objectives of this Dissertation Research

This dissertation aimed to investigate the mechanical and piezoelectric behavior of PZT in its composite form for MEMS. Uniaxial tension experiments to obtain full-field strains by digital image correlation (DIC) were employed to compute the stress vs. strain curves of individual and composite thin films such as SiO_2, SiO_2-Pt, SiO_2-Pt-PZT, and SiO_2-Pt-PZT-Pt. The mechanical properties of PZT were then derived from the composite properties of freestanding film stacks consisted of combinations of SiO_2, Ti, Pt, and PZT. Finally, the piezoelectric behavior of the PZT composite was investigated using a multilayer beam bending analysis and the piezoelectric coefficient d_{31} was derived. Finally, the effect of pre-stress on the hysteresis response of the PZT composite films was studied to better understand the performance of PZT MEMS under different loads.

CHAPTER 2

MECHANICAL BEHAVIOR OF PZT THIN FILMS

PZT films are commonly fabricated as multimorphs in conjunction with SiO_2 and Pt by using a sol-gel method. Due to the difficulty in etching individual freestanding PZT films, experiments must be conducted with specimens made with various combinations of SiO_2, Ti, Pt, and PZT. In this work, thin film stacks of SiO_2-TiPt-PZT-Pt, SiO_2-TiPt-PZT, SiO_2-TiPt and individual SiO_2 specimens were fabricated with gauge length of 1,000 μm and widths of 50-100 μm. The mechanical response of the individual PZT films can be extracted from the stress vs. strain curves of the composite stacks by using the composite laminate theory and by assuming isostrain conditions since no delaminations are detected in post-failure SEM imaging.

In the present study, all specimens used to extract the mechanical response of PZT were fabricated on the same wafer and hence subjected to the same thermal history. Since a limited number of specimens of each kind were available, a reliable experimental method was needed to obtain the material properties by methods described in Sections 2.2 and 2.3. Individual Pt films were not tested in this work, because prior results from the work by Jonnalagadda *et al.* [47] from this group by were used in the analysis.

2.1 Materials and Experimental Methods

The thin film specimens tested in this research were designed at UIUC and were fabricated at the US Army Research Laboratory (ARL) in Adelphi, MD. The patterned samples were fabricated by a combination of chemical vapor deposition, physical vapor

deposition and chemical solution deposition on a silicon substrate followed by various etching techniques to obtain freestanding dog bone thin film samples as shown in Figure 2.1. The SiO_2 thin film was deposited by plasma-enhanced chemical vapor deposition (PECVD) followed by rapid thermal anneal at 700ºC for 60 sec in N_2 to remove the trapped hydrogen from the film. Next, a sputtered Ti/Pt bottom electrode for the PZT film was deposited at 500ºC. A fine layer of Ti with 5-10 nm thickness is commonly used as an adhesive layer.

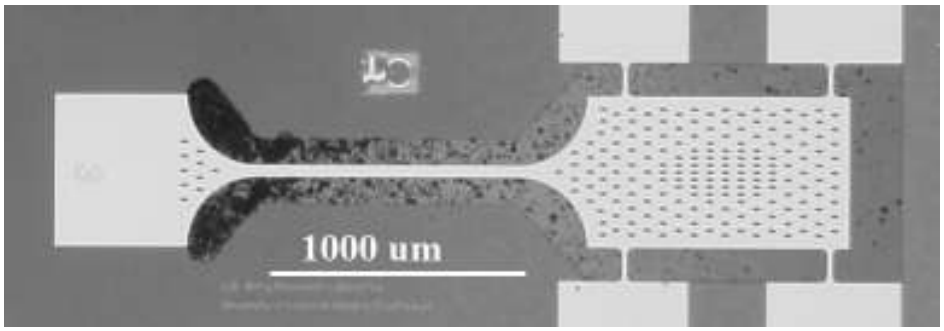

Figure 2.1 Freestanding SiO_2-TiPt-PZT-Pt film with one end fixed and other tethered to the silicon die.

The PZT thin films were prepared via chemical solution deposition motivated by the work by Budd *et al* [48]. A process schematic of the fabrication of the PZT composites is shown in Figure 2.2. The solutions had 12% excess lead to account for lead loss during the crystallization and were statically dispensed onto the wafer surface to be spun at 2,500 rpm forming an amorphous uniform coating. Pyrolysis at 350ºC was applied to remove most of the volatile organics. This spinning and pyrolysis procedure was repeated *four* times before the amorphous film was crystallized into PZT by using rapid thermal annealing at 700ºC in flowing oxygen to yield a film thickness of approximately 2,500 Å. This process was then repeated to achieve the target thickness of 10,000 Å. After annealing the PZT, a 1,050 Å Pt thin film was sputter-deposited directly onto the PZT surface at 300ºC.

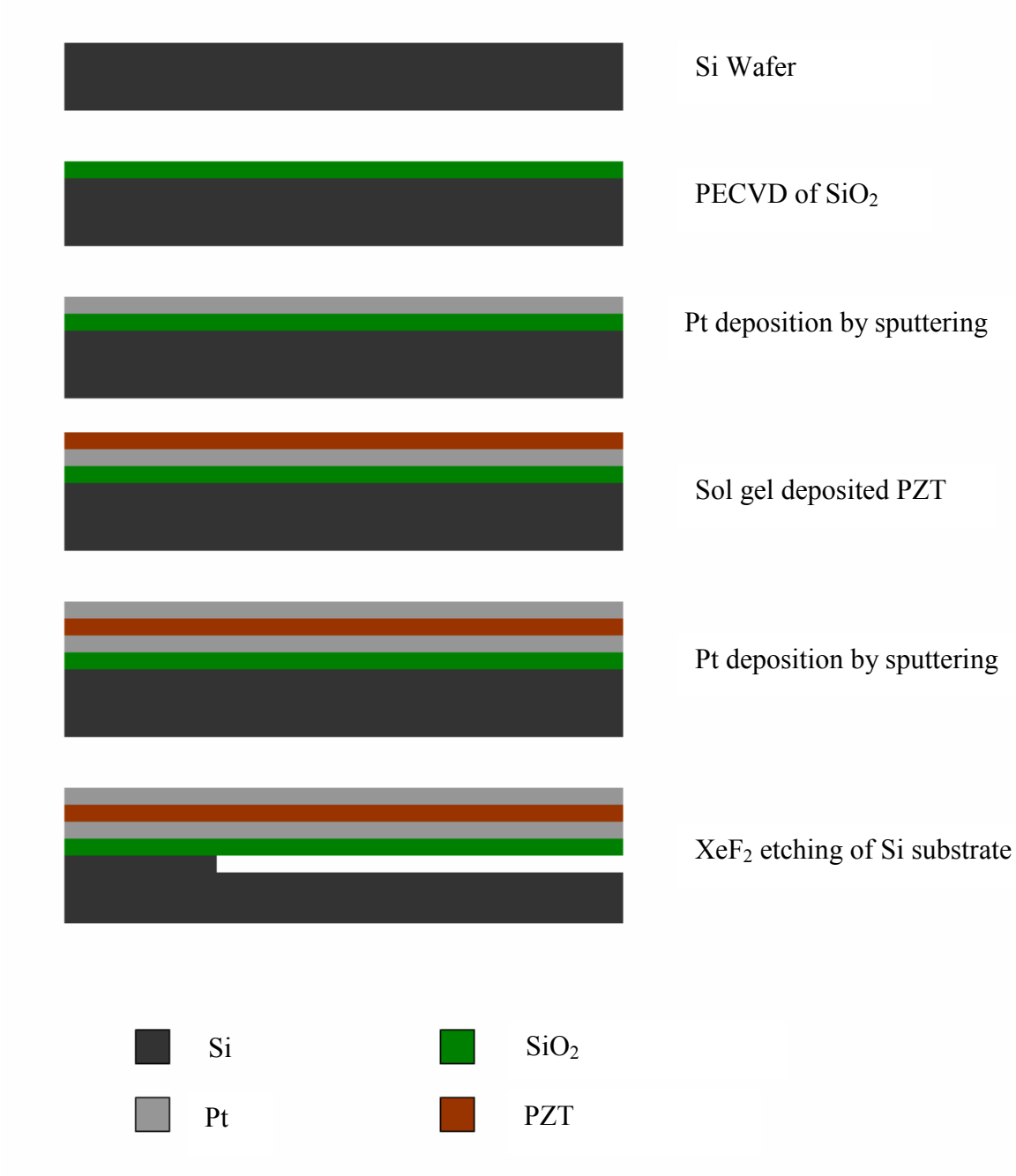

Figure 2.2 Process for PZT composite stack fabrication.

Subsequently, Ar ion-milling was used to first pattern the top Pt electrode, followed by another Ar ion-milling step to pattern the PZT and the Ti/Pt bottom electrode layers. Next, the exposed SiO_2 layer was patterned by reactive ion etch with CHF_3, CH_4, and He gases. The specimens were then partially diced out of the 100 mm wafer. The wafer with partial dicing streets was placed into a XeF_2 etching chamber. The XeF_2 was used to isotropically etch the Si to create freestanding "dog-bone" test structures as shown in Figure 2.1. One end of the specimen remained fixed to the substrate and the other was supported by tethers. The SiO_2 specimens had 1,000 μm gauge length, 50 μm or 100 μm width and 0.284 μm thickness. SiO_2-TiPt-PZT-Pt and SiO_2-TiPt-PZT stacks were of similar shape and gauge length but differed in their thickness due to an additional Pt layer, as shown later in Figure 2.7(a). Table 2.1 lists all the film combinations, and the residual stresses in each layer as measured by the ARL group using the wafer curvature method.

Table 2.1 Thickness and residual stress of PZT composite stacks tested in this work.

Layer	Layer thickness (nm)	Total thickness (nm)	Residual Stress (MPa)
SiO_2	280	280	29
SiO_2/TiPt	410/100	510	29/534
SiO_2/TiPt/PZT	410/100/1010	1520	29/534/48
SiO_2/TiPt/PZT/Pt	320/110/1070/120	1620	29/534/48/68

2.2 Experimental Methods

The uniaxial tension testing setup shown in Figure 2.3 consisted of a sturdy platform with a mounted PZT actuator to generate loading and a loadcell to measure the load in the sample, similar to that reported before [47,49,50]. The PZT actuator and the loadcell were mounted on translation stages that aided in specimen alignment with respect to the axis of the apparatus. The die containing the specimens was fixed onto a metal holder, connected to a loadcell. A glass grip, as wide as the specimen's pedal (600 μm), attached to the PZT actuator was bonded to the freestanding end of a specimen by a UV curable adhesive. The tethers supporting the specimen on the silicon wafer were broken by a sharp tungsten probe mounted onto a probing stage. The testing platform was placed under an optical microscope with a CCD camera to capture magnified (200×) pictures of the specimen's gauge section while loading. The specimens were loaded at a strain rate of $6 \cdot 10^{-4}$ s^{-1} and the load in the film was recorded by a loadcell. With the help of a very fine speckle pattern, the strain in the specimen was computed by DIC to plot stress-strain curves.

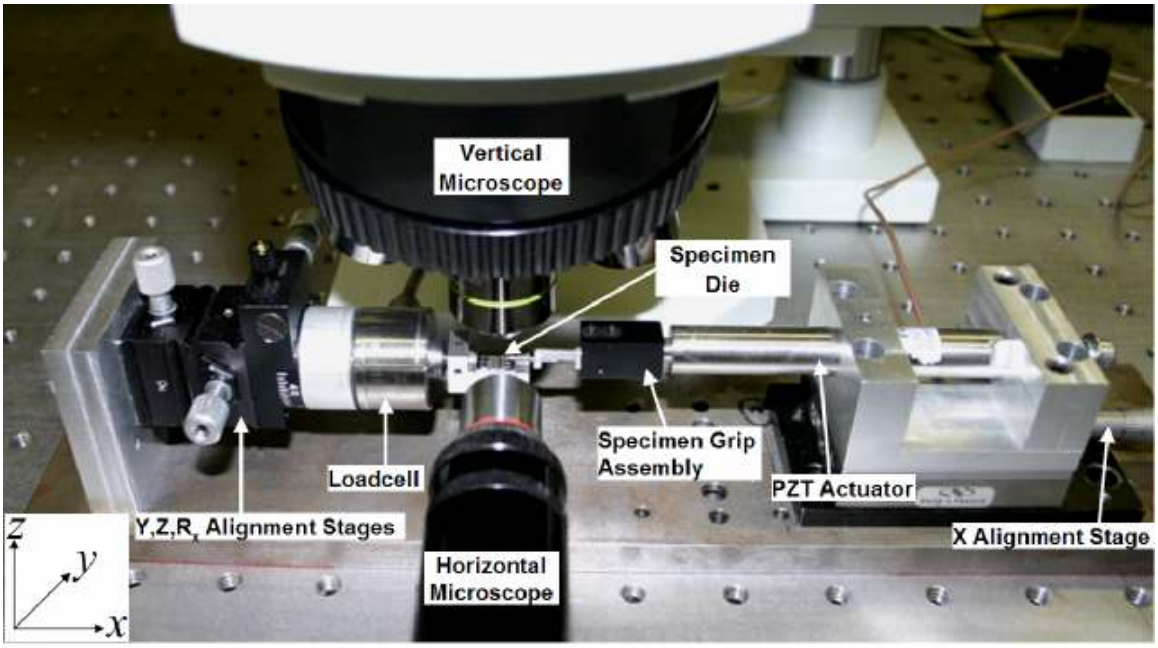

Figure 2.3 In situ microscale apparatus for uniaxial tension experiments [47].

Strain measurements were obtained directly from the specimen surface. Our group has already developed high resolution methods, such as the Atomic Force Microscopy/Digital Image Correlation (AFM/DIC) [49,50] to resolve strain fields directly from MEMS-scale specimens with widths as small as 6 μm. More recently, we reported on optical-based high resolution measurements of strain with the aid of DIC [47]. The latter approach was used in this work together with a fine speckle pattern deposited on the specimen surface, as seen in Figure 2.4(b).

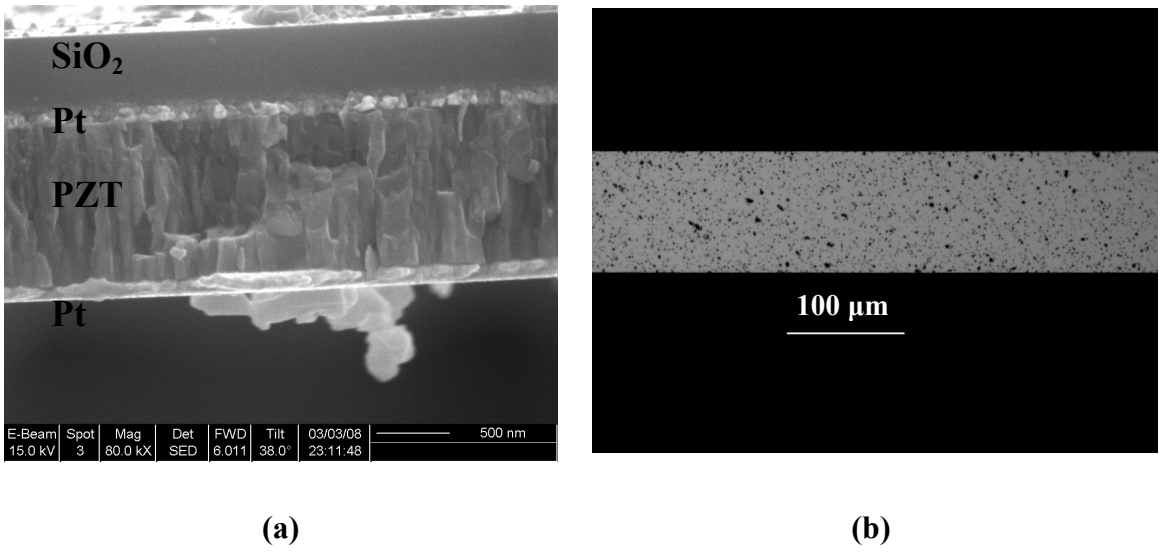

(a) **(b)**

Figure 2.4 (a) Cross sectional image of SiO_2-TiPt-PZT-Pt, and **(b)** specimen with fine speckle pattern for full-field strain measurements.

Developing such a dense pattern is challenging, due to the particles' natural tendency to agglomerate because of moisture or static charges, and the fact that the thin films are extremely fragile and cannot be exposed to wet conditions or a gas flow. Figure 2.5 shows a schematic of the apparatus designed to produce a dense and fine speckle pattern on the surface of freestanding specimens. The hollow cylindrical apparatus with closed bottom consisted of fine filters and inlets to introduce nanoparticles by compressed air. The die containing the "dog bone" shaped specimens was positioned in

an inverted manner at the top end of the cylindrical apparatus. Silicon nanoparticles were introduced into the cylindrical chamber through the powder inlet and compressed air was injected through the air inlet, randomly dispersing the fine nanoparticles to the specimen surface. This process was repeated several times to obtain the desired density of speckle pattern. Filters prevented the large particles from being deposited on the specimen's surface, which would deteriorate the resolution of the full field strains calculated by DIC.

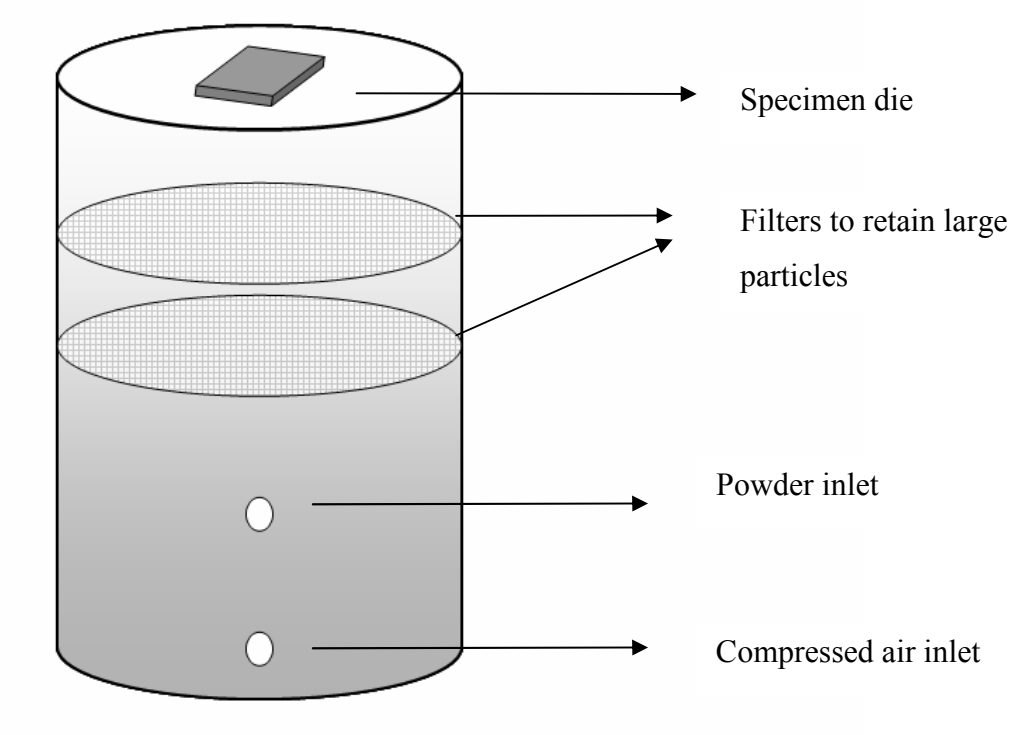

Figure 2.5 Apparatus to generate a speckle pattern on a freestanding thin film.

The speckle pattern with fine particles enabled testing at higher magnifications to enhance the strain resolution needed to calculate the Poisson's ratio of the different materials. To verify the quality of this speckle pattern, rigid body displacements of a Si wafer covered with Si particles were resolved by DIC and were compared to the motion induced by the PZT actuator. The specimen attached to the PZT actuator was displaced in steps of 12 nm over a total length of 1,200 nm while taking pictures of specimen's

surface by an optical microscope. A plot of the displacements calculated by DIC and those imposed by the PZT actuator is shown in Figure 2.6. Over this small range of displacements, the slope of the curve is very close to unity, while achieving 23 nm displacement resolution [51], which emphasizes the advantages of this patterning technique. This speckle pattern allowed us to measure both axial and transverse strains to calculate the elastic modulus and the Poisson's ratio of the materials at hand.

The Young's modulus of the specimens tested using the in-situ micro tensile testing apparatus was obtained by plotting the stress vs. strain data recorded during an experiment which were constructed from plots of the stress in the specimen as a function of time, as shown in Figure 2.7(a), and the strain as a function of time, as shown in Figure 2.7(b). A computer code was applied to match the strain and the corresponding stress values to construct the stress vs. strain plots as shown in Figure 2.7(c). The cross-sections of the fractured specimens were imaged by an SEM to measure the actual film thickness which differed from the nominal thickness calculated from the material deposition time.

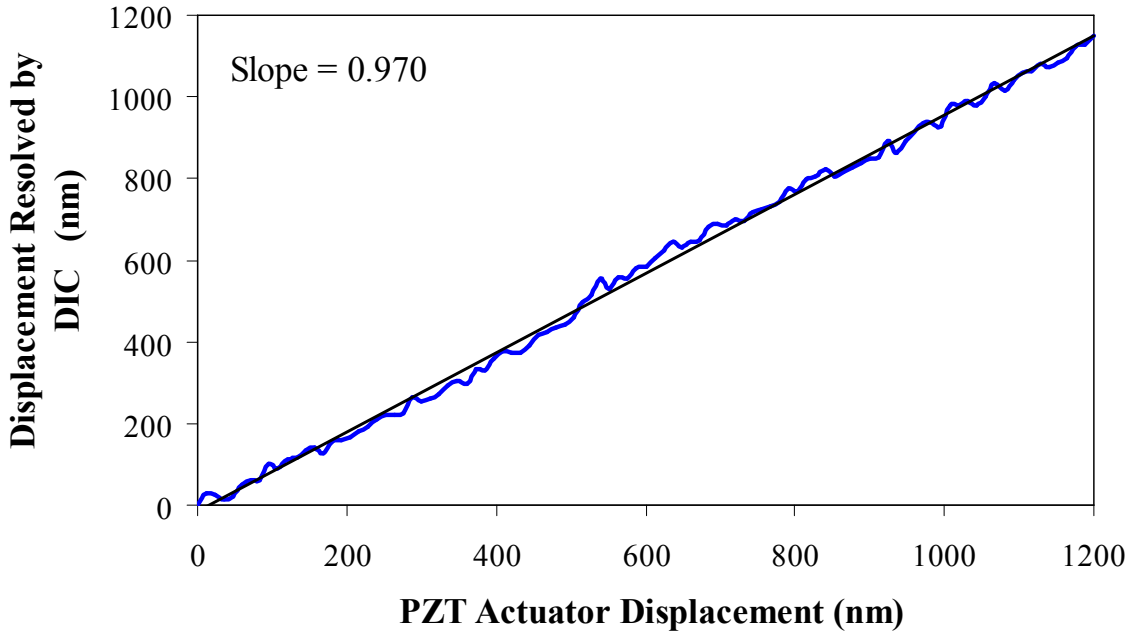

Figure 2.6 Comparison of rigid body motions imposed by a PZT actuator and those resolved by application of DIC.

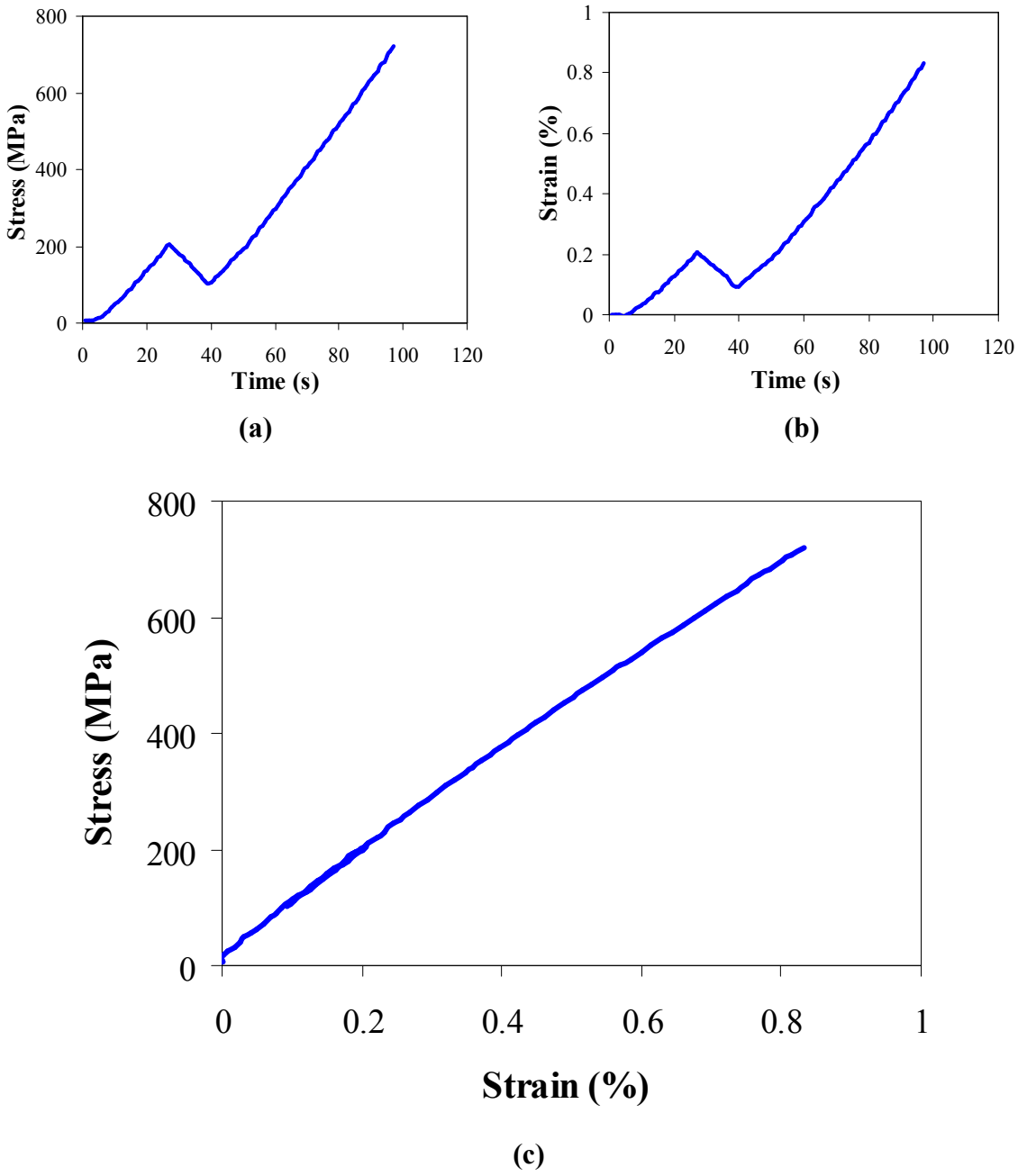

Figure 2.7 (a) Applied stress and **(b)** strain as a function of time. **(c)** Stress vs. strain plot for a PZT composite specimen derived by matching plots (a) and (b).

2.3 Results and Discussion

From the experimental data, we computed the stress-strain curves from which basic mechanical properties, such as elastic modulus, tensile strength and ultimate strain were calculated for SiO_2, SiO_2-TiPt, SiO_2-TiPt-PZT-Pt, SiO_2-TiPt-PZT films. The elastic modulus of PZT was extracted from the results for the composite films and previous data obtained by our group for Pt [47].

2.3.a Experiments with SiO_2 Thin Films

A total of eleven SiO_2 specimens were tested and their stress vs. strain curves were consistent in terms of linearity and modulus. Figures 2.8(a,b) show typical axial and transverse displacement fields for the SiO_2 specimens. It should be noted that the axial and the transverse displacement contours were very well aligned with the specimen direction which denotes the excellent alignment of the specimen in the tensile apparatus. An example stress vs. strain curve is shown in Figure 2.8(c). The as-fabricated specimens were slightly curved out-of-plane along their length due to a small pre-stress and hence measuring the film strain starting from a load-free state was not possible. However, the SiO_2 films showed excellent elastic behavior, as evidenced from the stress-strain plots, and outstanding ultimate strain which was considerably larger than bulk glass.

The elastic modulus of SiO_2 was measured as 72.3±2 GPa which agreed very well with the modulus of bulk silicon oxide of 73 GPa. The maximum stress was 1.1 GPa at a maximum strain of 1.6%, which is large compared to typical failure strains of brittle materials, and it is attributed to the small defect density of the SiO_2 films and the very smooth specimen edges. The failure strain was not the same for specimens from all wafers: for some wafers, the specimens broke at strains as low as 1.2% but the average failure strain was 1.4±0.2 %, see Table 2. However, the failure strengths of specimens fabricated in the same lot were very consistent. Strain in the lateral directions was also computed by DIC to calculate the Poisson's ratio of SiO_2, as shown in Figures 2.8(b,d). This is the first time that the Poisson's ratio of SiO_2 was measured from microscale

specimens and was found to be $\nu = 0.20$, which compared well with the bulk value of $\nu = 0.18$. The initial negative Poisson's ratio was due to specimen's curvature along width that appeared as high positive strain in the beginning of loading, but the calculated Poisson's ratio assumed a constant value when the specimen became flat.

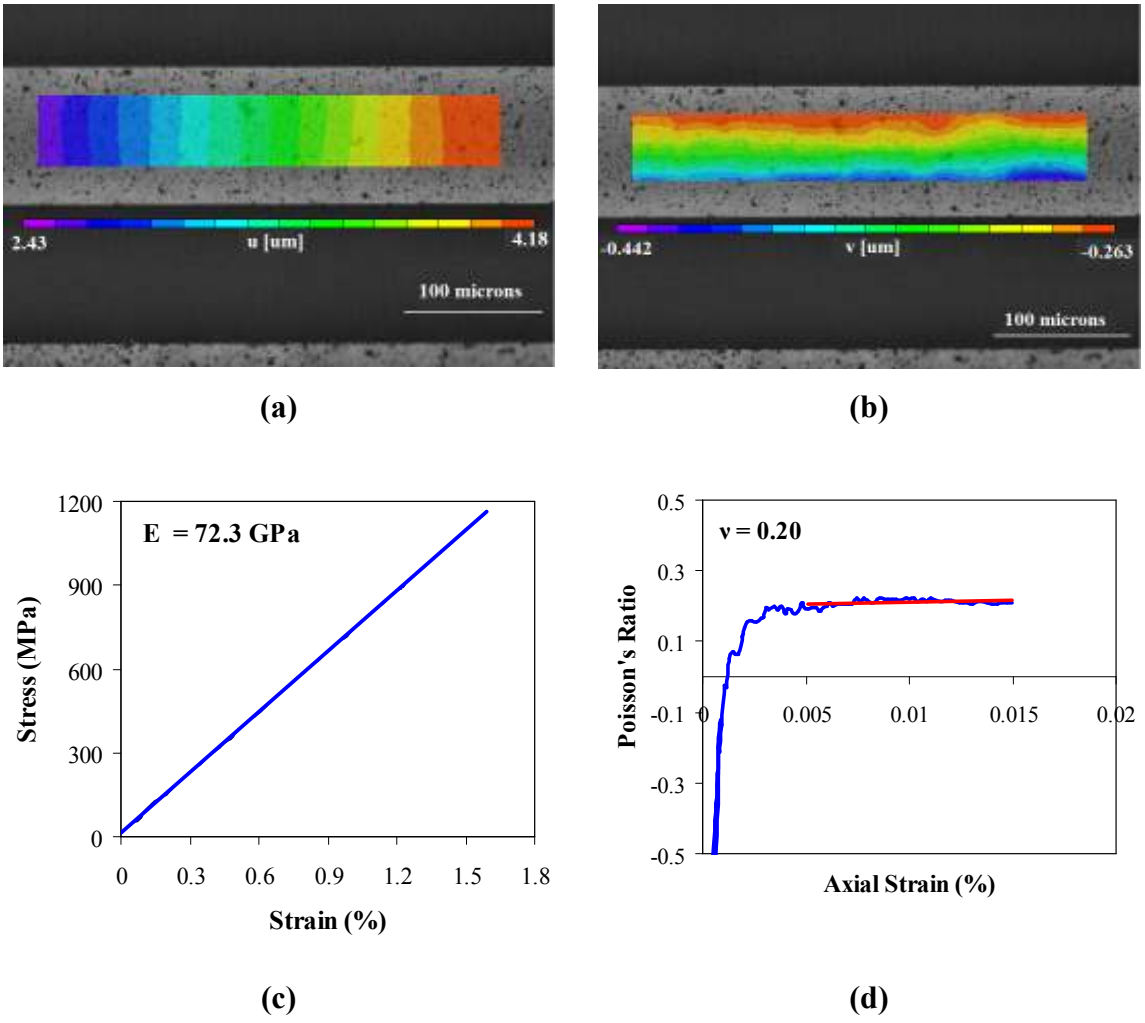

Figure 2.8 (a,b) Contour plots of axial and transverse displacement distributions, **(c)** stress-strain plot of freestanding SiO_2 film and, **(d)** Poisson's ratio plotted against axial (elastic) strain. The deviation at smaller strains is due to a slight curvature in the transverse direction that is removed as the specimen is axially loaded.

2.3.b Experiments with SiO_2-TiPt Composite Films

SiO_2-TiPt thin films were fabricated by sputter depositing a Pt layer on top of a SiO_2 thin film. The mechanical response of this composite film, calculated using simple laminate theory, is shown in Figure 2.9, which indicates the expectation for inelastic deformation beyond the elastic limit of Pt (0.6% strain) [47]. However, the experimental stress strain curve of SiO_2-TiPt was perfectly linear as shown in the same figure with an elastic composite modulus of 87.9 GPa, failure strength of 787 MPa and failure strain of 0.8% (for the particular specimen).

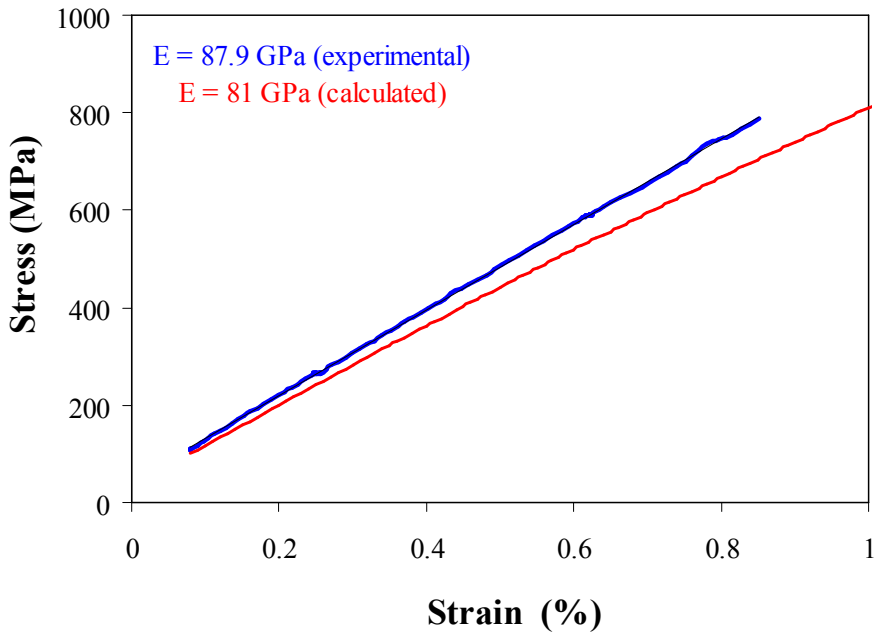

Figure 2.9 Experimental and predicted stress strain curve for SiO_2-TiPt films.

Even though Pt itself undergoes plastic deformation at 0.6% strain [47], the stress vs. strain curve of SiO_2-TiPt exhibited linear behavior until failure at 0.8% strain, which indicates delayed yielding of Pt because of its confinement by SiO_2. As the two layers are bonded firmly, the plastic deformation of Pt is constrained by the much thicker SiO_2 layer

thereby preventing Pt yielding. At higher loads, local deformation in the Pt film occurred and a sudden increase in stress in the (highly stressed) SiO_2 layer leaded to brittle failure that resulted to shattered films. Due to this failure mode, the investigation of fracture surfaces was not possible. However, cross-sectional SEM images were taken on the broken specimen tabs to identify possible delamination. The stress of individual layers in the composite was calculated with laminate theory assuming isostrain condition. At failure, the stress in the SiO_2 and Pt layers was 600 MPa and 2,000 MPa respectively after accounting for residual stresses in each layer according to Table 1. The stress in SiO_2 was always less than its average failure strength of 1,170 MPa discussed in Section 2.3.a, while the stress in the Pt layer was within its failure strength of 1,800-2,000 MPa [47]. Therefore, it is concluded that failure always initiated in the Pt layer. A summary of the average property values for this composite stack is given in Table 2.

2.3.c Experiments with PZT Composite Stacks

The stress vs. strain plots of PZT film stacks consisting of SiO_2-TiPt-PZT-Pt and SiO_2-TiPt-PZT are shown in Figure 2.10. Each plot includes an elastic loading-unloading segment and the final reloading to fracture. The composite moduli for the particular SiO_2-TiPt-PZT-Pt and SiO_2-TiPt-PZT films were 94.7 GPa and 87.8 GPa, respectively, with failure strains being 0.65% and 0.5%, respectively. The difference in the failure strain is attributed to the additional layer of strong Pt (see Figure 2.10) in SiO_2-TiPt-PZT-Pt. The average composite properties for both film stacks are listed in Table 2.

The stress vs. strain curves for all SiO_2-TiPt-PZT-Pt and SiO_2-TiPt-PZT specimens showed nonlinear behavior after approximately 0.35% strain. The subsequent nonlinear behavior was not attributed to plastic deformation of the Pt layer because the SiO_2-TiPt composite films did not exhibit nonlinear behavior as explained in Section 2.3.b.

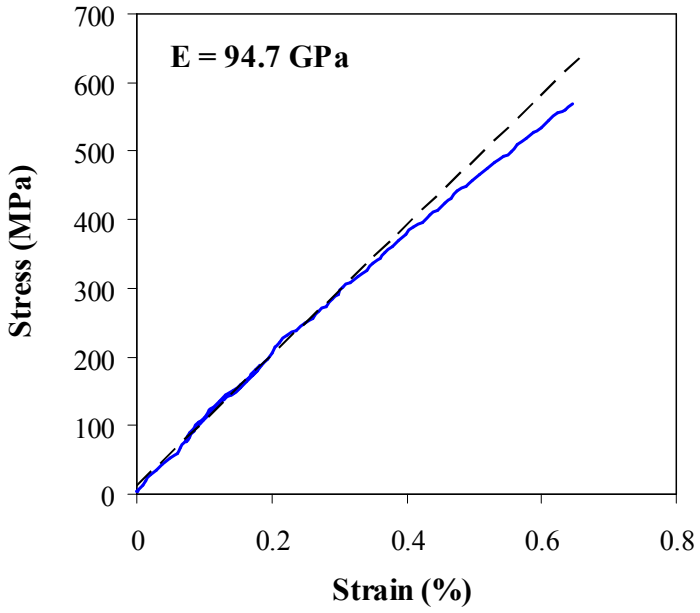

(a)

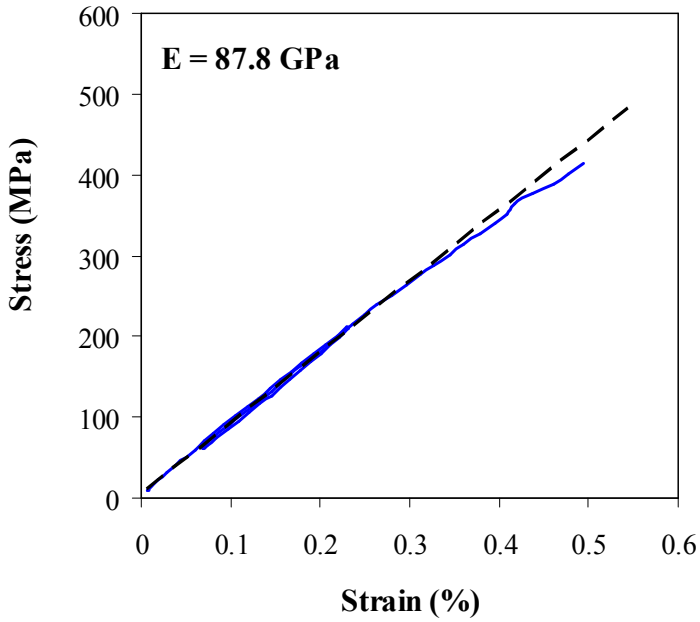

(b)

Figure 2.10 Stress vs. strain plot of a freestanding **(a)** SiO_2-TiPt-PZT-Pt and **(b)** SiO_2-TiPt-PZT film. Both plots include the loading-unloading and final reloading segments.

Further investigation was conducted on the PZT composites to understand their nonlinear behavior. Firstly, uniaxial tension experiments were carried out on both PZT composite stacks to deduce the presence of any inelastic deformation by performing multiple loadings (beyond 0.35% strain), unloadings to zero strain and a final reloading to failure. A stress vs. strain curve of a SiO_2-TiPt-PZT-Pt composite specimen for multiple loadings, unloadings and a final reloading is shown in Figure 2.11. As clearly shown, there was no deviation from one curve indicating a nonlinear elastic behavior of the PZT composite stacks. In literature, it has been reported that PZT exhibits nonlinear elastic behavior attributed to 90° domain switching upon applying stress [52,53], which is a possible explanation for the non-linear mechanical behavior recorded in the present stress vs. strain curves. Actually, due to its nonlinear elastic behavior, the elastic modulus for bulk PZT is often expressed in two different forms, namely the tangent modulus and the secant modulus. [54,55]. Subsequently, the PZT composite films were subjected to fatigue at various mean stresses and amplitudes at 50 Hz frequency. However, no failure was observed until more than 9 million cycles, at stress amplitudes ranging from 50-300 MPa and operated at a mean stress of 300 MPa and 400 MPa. This further supported the aforementioned conclusion that the present PZT composite films did not show an elastic limit but exhibited nonlinear elastic behavior.

The properties of PZT films in the linear regime (≤ 0.3% strain) were extracted from the mechanical response of the SiO_2-TiPt-PZT-Pt and SiO_2-TiPt-PZT composite films by simple laminate theory. PZT stacks fabricated by a combination of physical and chemical vapor deposition, along with chemical solution deposition of the different layers, have strong interfacial bonds that, upon uniaxial loading, subject all laminas to an isostrain condition. This is an assumption in the following calculations, which was supported by SEM images (Figure 2.4(a)) where no interlayer failure was detected. The total tensile load applied to the SiO_2-TiPt-PZT-Pt specimens was carried cumulatively by all layers leading to the following equation for the elastic modulus of PZT:

$$E_{PZT} = \frac{E_{Stack}t_{Stack} - \left(E_{SiO_2}t_{SiO_2} + 2E_{Pt}t_{Pt}\right)}{t_{PZT}} \tag{2.1}$$

where E and t are elastic modulus and the thickness of each layer in the subscripts. A Ti layer measuring a few nanometers was used as adhesive material between SiO_2 and Pt, but because of its small thickness and its propensity to diffuse into each of the surrounding layers it was not taken into account in the calculation of the PZT properties. The thickness of the individual layers of the composite was measured by cross-sectional SEM imaging, as shown in Figure 2.4(a). It was found to vary in different dies and fabrication lots, and it was quite different from the nominal values estimated by deposition rates and times.

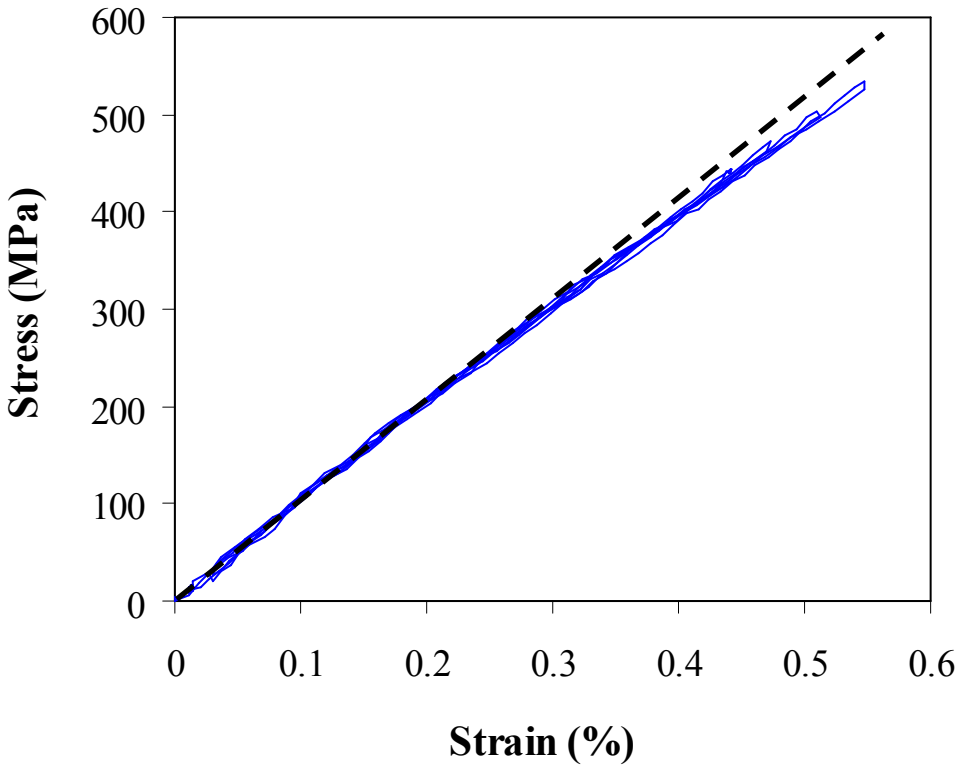

Figure 2.11 Stress vs. strain curve of SiO_2-TiPt-PZT-Pt composite under multiple loadings, unloadings and a final reloading. Note the deviation from linearity at ~300 MPa.

Similarly to the full PZT composite stack, the following equation was used to compute the PZT modulus from experiments on the composite stack SiO_2-TiPt-PZT:

$$E_{PZT} = \frac{E_{Stack}t_{Stack} - \left(E_{SiO_2}t_{SiO_2} + E_{Pt}t_{Pt}\right)}{t_{PZT}} \tag{2.2}$$

Substituting the values for the moduli measured for SiO_2, SiO_2-TiPt-PZT-Pt and SiO_2-TiPt-PZT and for Pt (E=173.2 GPa) from reference [47] in Equations (2.1) and (2.2), the average elastic modulus of the PZT in each stack was 82.4 GPa and 85.3 GPa, respectively, giving an average of 84±2 GPa. The mechanical properties of all materials tested are listed in Table 2.2. Figure 2.12 shows a comparison of the different stress vs. strain plots for each (composite) layer. Equations similar to (2.1) and (2.2) were used to calculate the failure strength of PZT assuming fracture was initiated in the PZT layer. This is supported by the fact that the failure strain of SiO_2 was systematically higher than that of the composite stacks. By virtue of a maximum principal strain criterion it is deduced that PZT was the weakest link in all composite films. The average tensile strength of the PZT layer was 510±35 after accounting for residual stresses from Table 1.

Table 2.2. Mechanical properties of the PZT composites.

Material	Modulus (GPa)	Failure Stress (MPa)	Failure Strain (%)
SiO_2	72.3±2	1,060±200	1.4±0.2
SiO_2-TiPt	87.9±1	780±70	0.8±0.1
Pt [47]	173	1,876±10	3.84±0.26
SiO_2-TiPt-PZT	87.9±1	412±50	0.5±.0.05
SiO_2-TiPt-PZT-Pt	93.5±6	511±50	0.6±0.05
PZT (Extracted)	84±2	510±35	0.5±0.1

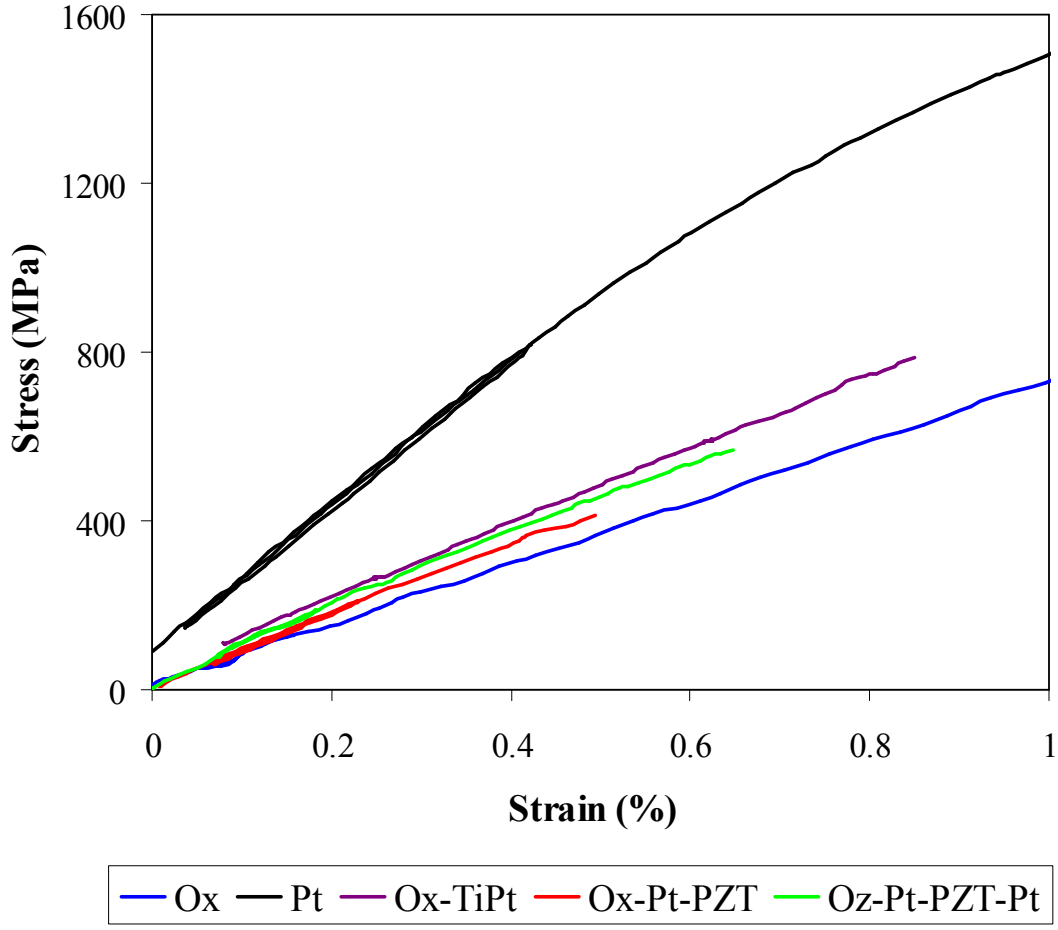

Figure 2.12 Stress vs. strain curves of the different layers in the PZT stack. All curves include the loading-unloading and final reloading segments. The Pt curve was adopted from reference [47].

2.4 Conclusions

In this Chapter, the mechanical properties of PZT film stacks with different combinations of SiO_2, Ti, Pt and PZT were reported for the first time. The elastic modulus of freestanding SiO_2 films was found to agree very well with bulk measurements, E= 72.3±2 GPa, with average maximum tensile strength and strain of 1,060±200 MPa and 1.4±0.2%, respectively. The Poisson's ratio of SiO_2 was measured for the first time from thin films and was found to be 0.20, which also agrees well with reported values for bulk SiO_2. The stress vs. strain curves of SiO_2-TiPt thin films were linear with an average failure strain of 0.8% and elastic modulus of 87.9 ±1 GPa. At failure, strain localization or cracking in the Pt layer, due to the layer stress exceeding its fracture strength, initiated failure leading to brittle fracture of the composite. On the other hand, the failure strength of the SiO_2-TiPt-PZT-Pt and SiO_2-TiPt-PZT composites was in the range of 410-510 MPa. From the stress-strain curves of the freestanding SiO_2-TiPt-PZT-Pt and SiO_2-TiPt-PZT thin films, the average elastic modulus for PZT was 84±2 GPa and the average tensile strength was 510±35 MPa after accounting for residual stresses in the PZT layer. Both PZT stacks exhibited nonlinear elastic behavior beyond 0.35% strain, an important property to be considered during the design of MEMS devices. This non-linear behavior was owed to intrinsic domain switching in the PZT films and not to plasticity in the attached Pt layer that demonstrated delayed yielding.

CHAPTER 3

PIEZOELECTRIC BEHAVIOR OF PZT THIN FILMS

Piezoelectricity is exhibited by certain crystalline materials that generate electric charge proportional to an applied mechanical stress. Conversely, when exposed to an electric field, the same materials undergo mechanical deformation (strain). The former phenomenon is termed as the direct piezoelectric effect and the latter is called the inverse piezoelectric effect. This material property is being used in high voltage and power sources, sensors, actuators, frequency standard and piezoelectric motors. Due to the growing demand for miniaturized devices, microscale piezoelectric devices such as airbag sensors [56], MEMS microphone [57], RF switches [58] and accelerometers [59] for MEMS applications have been developed in the last two decades. Most of these MEMS devices include structures made of piezoceramic for either actuation or sensing purposes.

Piezoelectric MEMS, such as accelerometers and switches, are thin film PZT structures that have the advantage of being lightweight and compact and are preferred over conventional gyroscopes [60] and electromagnetic switches [61] because of their high force output and low voltage requirements. Unfortunately, the existing background on the piezoelectric behavior of bulk piezoelectric ceramics, such as $BaTiO_3$ and PZT, studied over the last century, is not appropriate to describe the response of thin film PZTs because the domain composition, grain size, defect chemistry and mechanical boundary conditions of thin film PZTs differ significantly compared to bulk PZT [62]. In this Chapter, the approach of multilayer beam bending was employed to quantify the piezoelectric behavior of the thin film PZT stacks described in Chapter 2.

3.1 Background on Piezomechanics

Natural materials such as quartz, tourmaline, Rochelle salt, etc., exhibit a weak piezoelectric behavior. Synthetic polycrystalline ferroelectric ceramics, such as barium titanate ($BaTiO_3$), lead titanate ($PbTiO_3$), lead zirconium titanate ($Pb[Zr_xTi_{1-x}]O_3$ $0<x<1$), and lithium tantalate ($LiTaO_3$) [63] outperform natural piezoelectrics. Of them, lead zirconium titanate, commonly known as PZT, is the most widely used piezoelectric ceramic today.

Piezoelectric ceramics, such as barium titanate and PZT, crystallize in the perovskite structure, which is a unit cell with large cations at its corners, a small cation at the body center and an anion at each face center. Above the Curie temperature, 190°-200° C [64], this perovskite structure is cubic but distorts to assume tetragonal structure below the Curie temperature, thus offsetting the smaller cation located at the body center. The unsymmetrical charge distribution in this tetragonal structure acts as a dipole resulting in net polarization in a particular direction while the unit cell exhibits piezoelectric behavior. In the case of a PZT unit cell, the Ti ion at the body center of the cubic structure is displaced as shown in Figure 3.1. Groups of unit cells with uniform polarization axis are called Weiss domains. Due to random distribution of domain orientations in a ceramic crystal no macroscopic piezoelectric behavior is observed. However, due to the additional ferroelectric nature of PZT, the polarization direction of different domains can be forcefully aligned by an opposing electric field above a certain field threshold.

A bulk PZT ceramic with permanent polarization is fabricated and then poled while heating the crystal beyond its Curie temperature followed by cooling while maintaining the electric field in the entire process. Figure 3.2 shows a schematic of the domain orientations during this process. However, sol-gel prepared PZT thin films are self-poled and do not require external poling to possess net remnant polarization [65]. This is illustrated in Figures 3.1 and 3.3 by using models of the perovskite unit cell subjected to various electric fields. The unit cell with displaced cation from body center with no applied electric field is shown in Figure 3.1(1). Under an electric field, the Ti cation shifts in the direction of the electric field by extending the unit cell vertically and

contracting it laterally, Figure 3.1(2). Upon reversal of the electric field to the *zero* value, a remnant polarization exists (due to the surrounding mechanical stresses) that is nullified by applying a coercive electric field E^c in opposite direction so that the unit cell shrinks in the vertical direction as shown in Figure 3.1(3). A reversed electric field greater than E^c shifts the body center cation in the opposite side as shown in Figure 3.1(4) during which the cell expands in the vertical direction. This is commonly referred to as *180° switching* of a domain and Figure 3.3 demonstrates an example of *90°* switching of a domain.

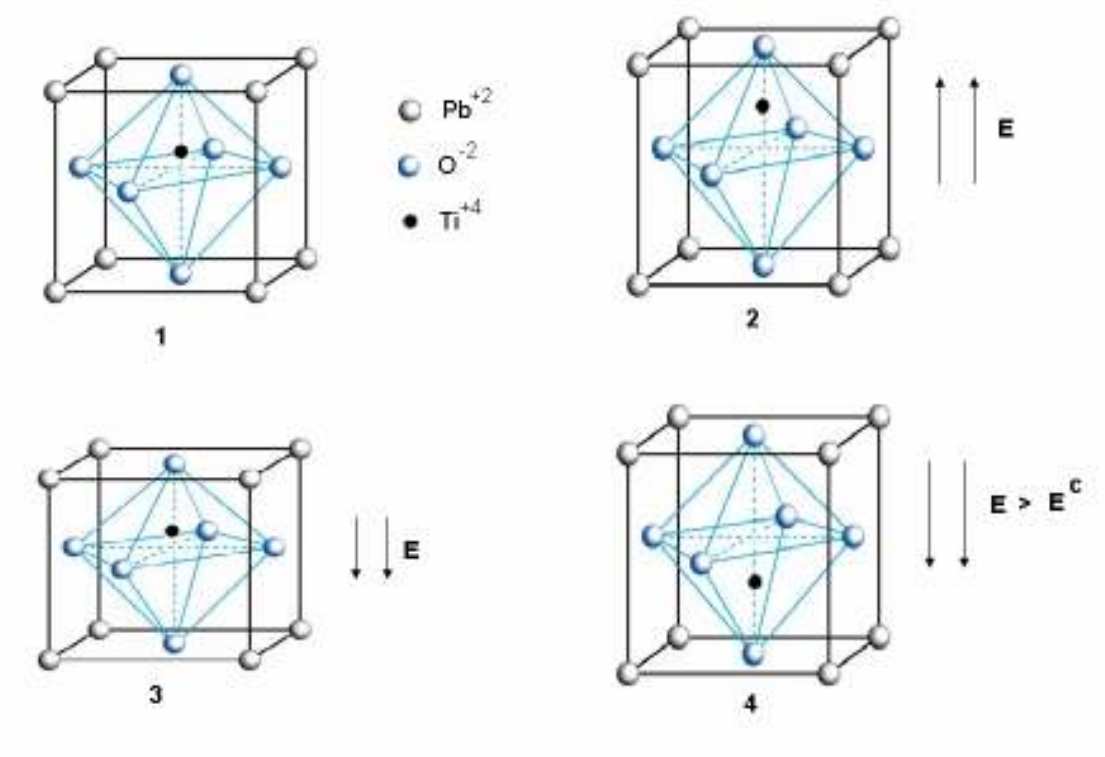

Figure 3.1 Perovskite unit cell structure below the Curie temperature. **(1)** No electric field, **(2)** electric field, **(3)** small reverse electric field, and, **(4)** reversed electric field greater than the coercive field. Redrawn from reference [66].

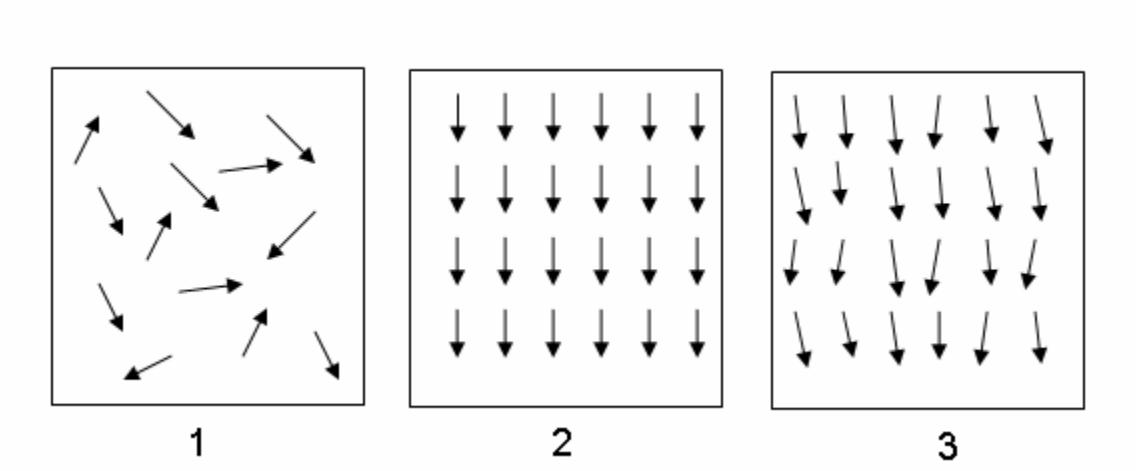

Figure 3.2 Electric dipoles domains in **(1)** unpoled piezoelectric ceramic, **(2)** during, and **(3)** after poling. Redrawn from reference [67].

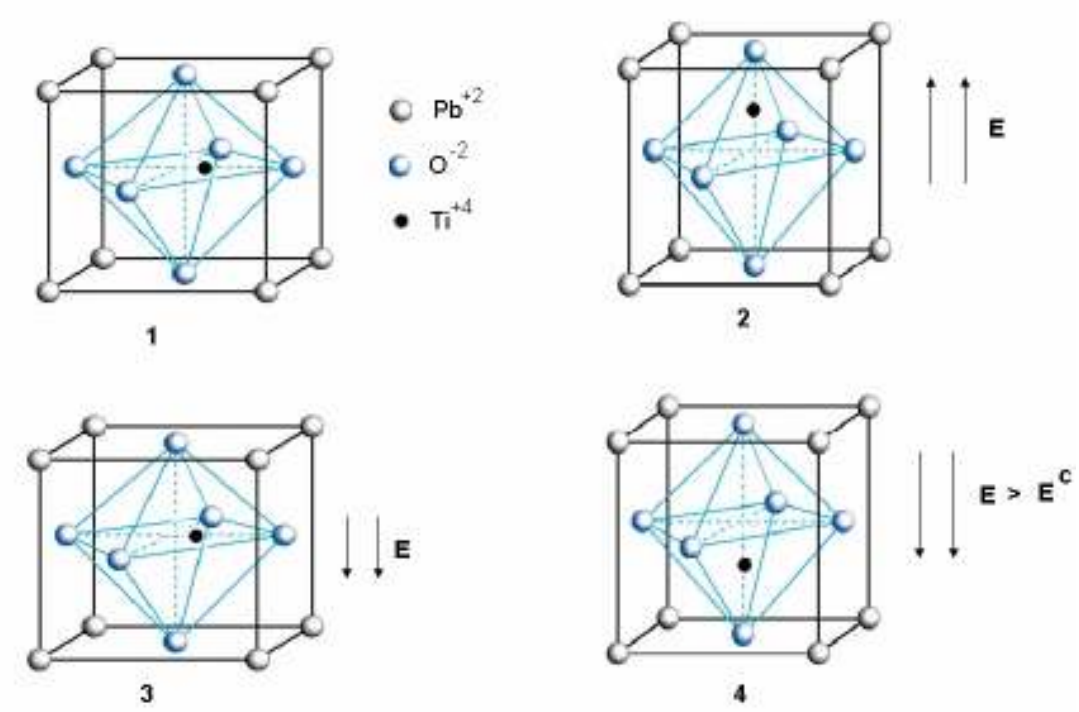

Figure 3.3 90° domain switching of Perovskite unit cell **(1)** no electric field, **(2)** upward pointing electric field, **(3)** small reverse electric field and, **(4)** reversed electric field greater than coercive field. Redrawn from reference [66].

The piezoelectric response of PZT ceramics is quantified via the piezoelectric coefficients d_{ij}. The interdependent relationship between the electric field E_j, the electric displacement D_i, strain and applied stress T_j is described by Equations (3.1) and (3.2), where ε_{ij} is the dielectric permittivity, d_{ij} is the piezoelectric coefficient tensor and S_i is the strain developed. While Equation (3.1) describes the direct piezoelectric behavior where electric potential is developed due to applied stress, Equation (3.2) describes the inverse piezoelectric effect which is commonly used for actuation purposes:

$$D_i = \varepsilon_{ij} E_j + d_{ij} T_j \tag{3.1}$$

$$S_i = d_{ij} E_j + s_{ij} T_j \tag{3.2}$$

Bulk PZT has been extensively studied to understand its piezomechanical properties, which, however, can be significantly different from that of thin films with the same composition [70-73]. In bulk materials, the piezoelectric properties such as dielectric constant, remnant polarization, and hysteresis are due to domain wall movement [74]. Recent studies on bulk materials showed that the material's microstructure affects the mobility of twin walls and, hence, the piezoelectric properties. It has been reported that the dielectric and piezoelectric properties are degraded for grain sizes smaller than 1 μm [74]. This has direct impact on the piezoelectric properties of PZT thin films since the grain size is often of the order of few hundred nanometers. Additionally, the stresses imposed by the adjoining layers such as electrodes for biasing or substrates can restrict the domain wall movement by firmly clamping them. Hence the piezoelectric behavior of the PZT thin films can be lower compared to their bulk counterparts [75]. This led to the investigation of fundamental differences between bulk and thin film perovskite structures, which are attributed to material thickness, grain size,

crystal orientation, and residual stresses [76-79]. Hence it is important to accurately determine the piezoelectric behavior of PZT material at the MEMS scale.

Different methods have been employed to quantify the piezoelectric coefficients, especially d_{33} and d_{31}, which determine the magnitude of the piezoelectric response. A schematic of a PZT ceramic under electric field is shown in Figure 3.4. The piezoelectric coefficient d_{31} signifies the induced in-plane strain per unit electric field applied perpendicularly to the film, while d_{33} stands for induced out of plane strain per unit electric field applied in the perpendicularly to the film. For a PZT material, the d_{31} and d_{33} values depend on the processing conditions, substrate material and poling conditions. Additionally, measuring the d_{31} and d_{33} values is challenging due to the fabrication of PZT as a composite film and hence, mechanical clamping of the thin film on the substrate and its electrodes can strongly influence its piezoelectric response.

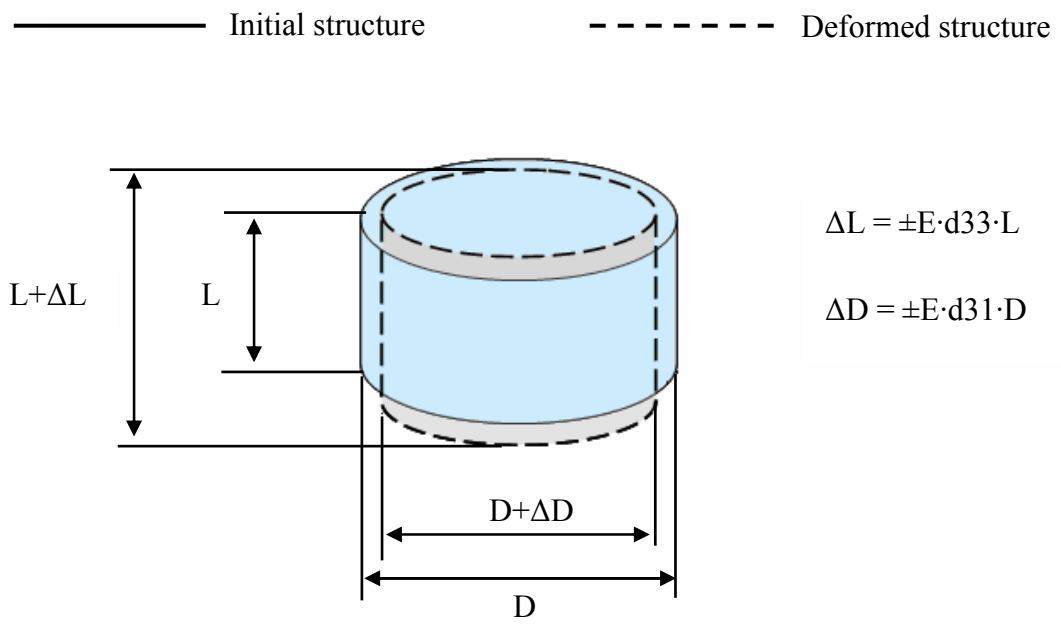

Figure 3.4 Piezoelectric ceramic element subjected to electric field. Redrawn from reference [66].

Most PZT actuators are driven in-plane [80] and hence the accurate measurement of d_{31} is desired. Various experimental techniques have been used to obtain the piezoelectric coefficients but there is a wide disparity among the d_{31} and d_{33} values reported, ranging from 30 pm/V to 220 pm/V and 29 pm/V to 400 pm/V, respectively [81-88] as shown in Table 3.1. Ayele *et al* [81] used double beam interferometry to measure the transverse piezoelectric coefficient d_{31} of PZT thin films integrated in multilayer silicon micro-membranes. The impact of DC voltage and buckling effects on d_{31} was studied and the measured values ranged from 30 to 75 pm/V. Scanning evanescent microwave microscopy capable of measuring 10 pm displacements was used by Zhao *et al* [82] to measure the piezoelectric coefficients of PZT thin films. The method used a scanning tip operating in non-contact mode at 1 μm above the sample with advantages of high scanning speed, large scanning area and high spatial resolution. The maximum d_{31} value was 220 pm/V while operating at 9 MV/m. In another study, Ong *et al* [87] reported an increase in the dielectric constant with reduction in residual stress. They measured the d_{33} coefficient in the range of 30-45 pm/V by using single beam heterodyne laser interferometer. The residual stress effect on the piezoelectric behavior of sol-gel prepared PZT thin films was also investigated by Berfield et al [88]. A single beam heterodyne laser interferometer was used to measure the field induced strain hysteresis loop. Interestingly, a drop in the piezoelectric response of these films at higher residual stresses was reported. While the d_{33} coefficient was in the range 29-65 pm/V, the higher values corresponded to films with lower residual stresses. This behavior was attributed to a reduction in polarization switching and domain motion at higher residual stresses in the film. Although it was reported that the piezoelectric coefficients for the PZT thin films are lower compared to the coefficients for bulk PZT (93.5 pm/V and 223 pm/V for d_{31} and d_{33} respectively [63]), some of the values reported were significantly higher than the corresponding values for bulk PZT. The scatter in the reported values can be attributed to the difference in fabrication techniques, which may result in values that differ by a factor of 10 or more [89]. A summary of the piezoelectric coefficients for different fabrication methods is provided in Table 3.1.

Table 3.1 Summary of piezoelectric coefficients reported for PZT thin films.

Material and Fabrication Method	d_{31} (pm/V)	d_{33} (pm/V)
Bulk PZT [63]	93.5	223
Sol-gel deposited PZT thin film [83,84,86-88]	84-220	29-400
Aerosol deposited [85]	80-180	N/A
RF Magnetron sputtered [81]	30-75	N/A

However, much is still unknown about the theoretical calculation and the measurement of electrically induced strains in layered PZT composite materials. In this dissertation, thin film composites made of PZT sandwiched between Pt electrodes with an attached SiO_2 layer were tested to measure d_{31}. The PZT specimens were fabricated on a silicon wafer and were released to their freestanding state, in which they were fixed at one end on the silicon wafer. Upon application of an electric field, the specimens bent out-of-plane which made difficult the measurement of the piezoelectric coefficients through conventional methods. Instead, the multilayer beam bending method [90] was used to compute d_{31} by measuring out of plane deflection of the PZT films to calculate the coefficient d_{31} by using a literature model.

3.2 Measurement of Piezoelectric Coefficient d_{31}

The composite PZT specimens used to evaluate d_{31} were identical to the dog boned shaped specimens described in Chapter 2 and shown in Figure 2.1. When an electric field was applied across the PZT layer, its domains aligned parallel to the electric field thereby inducing negative in-plane strain. Due to uneven stresses developed in the composite PZT beam, it underwent out-of-plane bending, similarly to a bimetallic strip

subjected to thermal stresses. Then, the analytical model of a piezoelectric beam subject to bending developed by Balls *et al* [90] was used to compute the d_{31} piezoelectric coefficient. However, their closed form solutions are applicable to cantilever beams with uniform cross-section. Hence, as shown in Figure 3.5 below, a thin glass beam was attached to the specimen neck to firmly bond it to the substrate and effectively make it a cantilever beam with uniform cross-section.

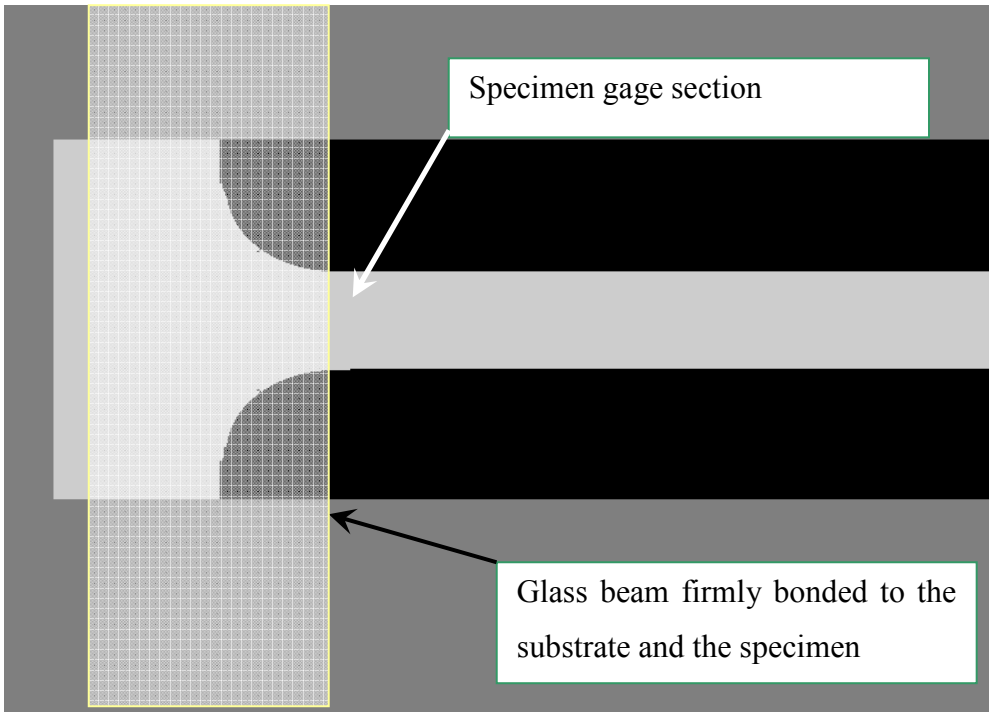

Figure 3.5 Thin film PZT cantilever specimens tested to measure d_{31}.

A micropositioner with an electrically conducting probe, connected to a DC power supply with a voltage regulator, were used to bias the Pt electrodes in the composite at a location that was firmly bonded to the substrate. The dies were mounted vertically under an optical microscope as shown in the Figure 3.6. Optical images of the specimen's sidewalls were recorded to measure the beam deflection upon application of an electric field. The as fabricated samples did not have a patterned circuit to bias the Pt

electrodes. Instead, the top Pt layer was connected via a probe directly while the sandwiched Pt electrode was accessed by electrically melting the top Pt layer in a small region by resistive heating. This enabled a sharp probe to make electrical contact with the second Pt electrode. Optical images of the specimen's cross section were taken at different bias voltages ranging between 0-8V (see later Figure 3.8). These images were later analyzed to calculate the deflection of the beam based on pixel count.

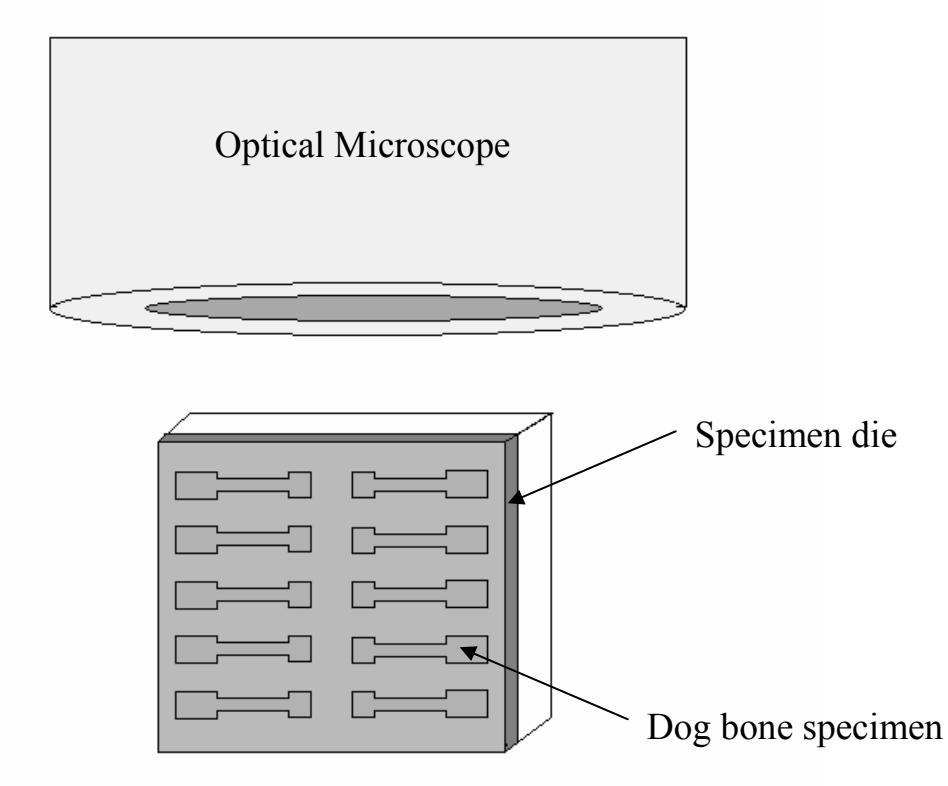

Figure 3.6 Schematic of a die containing PZT specimens placed vertical under optical microscope to measure the out-of-plane deflection of the PZT stacks due to an applied voltage.

Closed form equations for the bending response of a clamped-free piezoelectric multilayer beam subject to various excitations at any point along the beam were formulated by Ballas *et al* [90]. These equations were presented in a 4×4 matrix that combined the boundary conditions such as a mechanical moment at the end of the beam, a perpendicular force applied at the tip or a uniform pressure, and an applied voltage with the beam deformation geometry such as angular deflection, tip deflection and electric charge. In their study, the neutral axis, the moment due to the piezoelectric behavior of the PZT and their effect on the bending response of the neutral axis were considered in deriving the equations. It was assumed that the layers contained in the composite are either piezoelectric or elastic, are firmly bonded to each other such that no delamination occurs, the radius of curvature of the beam undergoing bending is much larger than its thickness and finally, the width of the beam is much larger than its thickness. The PZT composite thin film was composed of individual layers with different material properties and thickness; hence the location of the neutral axis was not at the composite beam's mid-plane. For the multilayered beam in Figure 3.7 the position of the neutral axis $\bar{z}$ was calculated by using Equation (3.3), where w_i, h_i, and $S_{11,i}$, represent the width, thickness and the compliance of the i^{th} layer, respectively:

$$\bar{z} = -\left(\frac{\sum_{i=1}^{n} \frac{w_i}{S_{11,i}} h_i^2 - 2\sum_{i=1}^{n} \frac{w_i}{S_{11,i}} h_i \sum_{j=1}^{i} h_j}{2\sum_{i=1}^{n} \frac{w_i}{S_{11,i}} h_i} \right) \tag{3.3}$$

With an electric field E applied in z direction, the beam deflection ξ at any location on the beam is described by

$$\xi = \frac{U m_{piezo} l^2}{2C} \left(\frac{x}{l} \right)^2 \tag{3.4}$$

where m_{piezo} and C are given by the following equations:

$$m_{piezo} = \frac{1}{2}\sum_{i=1}^{n}\frac{w_i d_{31,i}}{S_{11,i}h_i}\left[2zh_i - 2h_i\sum_{j=1}^{i}h_j + h_i^2\right] \tag{3.5}$$

$$C = \frac{1}{3}\sum_{i=1}^{n}\frac{w_i}{S_{11,i}}\left[3h_i\left(\bar{z} - \sum_{j=1}^{i}h_j\right)\left(\bar{z} - \sum_{j=1}^{i-1}h_j\right) + h_i^3\right] \tag{3.6}.$$

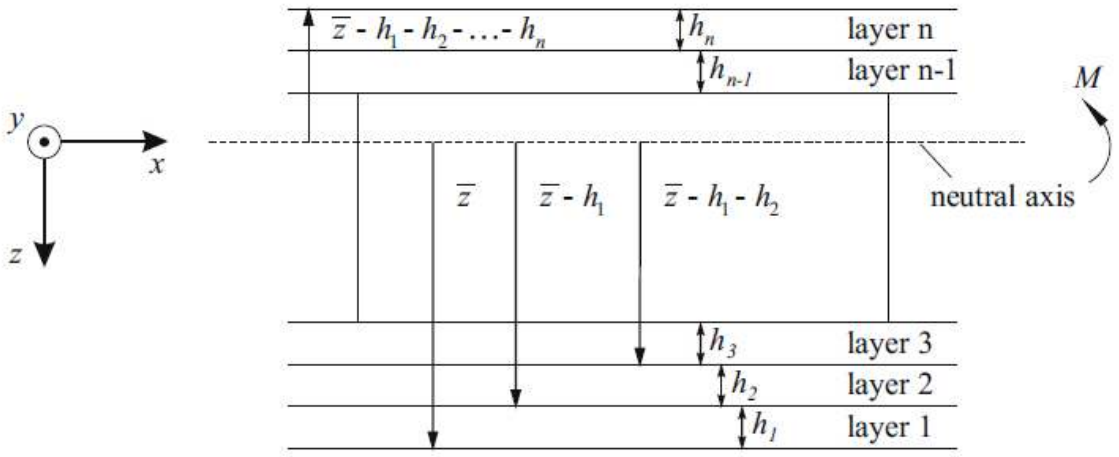

Figure 3.7 Schematic of a multilayered beam used in [90] to derive Equations (3.3) – (3.6). Image adopted from reference [90].

3.3 Results and Discussion

Optical images of the beam's profile taken at different bias voltages between 0-6 V are shown in Figure 3.8. The stress mismatch between the PZT layer and the attached Pt and SiO_2 resulted in greater composite beam deflection up to 480 μm. The piezoelectric coefficient d_{31} was calculated as 385±45 pm/V pm/V by using equations (3.3) - (3.7). This d_{31} value is much higher than that reported for bulk PZT [63] (93.5 pm/V) and is significantly higher (by a factor of 2) than the maximum d_{31} value reported in literature for sol-gel prepared PZT thin films. This may be attributed to the presence of fewer defects, lack of microcracking, perfect bonding between layers and the influence of fabrication conditions in the formation of PZT with high ferroelectric properties. However, the fact that this value is obtained from only one test prevents us from drawing concrete conclusions and hence, further work is required to obtain statistical measurements for d_{31}.

Additionally, the effect of an applied pre-stress on the electric field induced stress hysteresis of the PZT composite film was measured. The in-situ microscale tensile testing apparatus described in Chapter 2 was used to preload the specimens that were then biased with a DC voltage varying between -10 V and 10 V. The force on the specimens was recorded by the loadcell attached at one end of the specimen while the other end was firmly attached to an actuator. Because the loadcell is insensitive to bending loads, the load recorded is a measurement of the axial load in the specimen due to the contraction of the PZT layer. The electric field induced stress is plotted against applied voltage in Figure 3.9. The field induced stress hysteresis loops were asymmetric at small applied stresses becoming of equal magnitude as the applied stresses larger than ~350 MPa, before accounting for residual stresses in the PZT layer. Residual and mechanical stresses do affect domain switching in piezoelectric ceramics [63,91]: at higher stresses, the domains that could easily undergo 90° switching in the direction that cause hysteresis on the right half of butterfly loops are mechanically constrained. This leads to reduced hysteresis in the right half of the butterfly curve thereby making the hysteresis loops equal in magnitude.


0 V


1 V

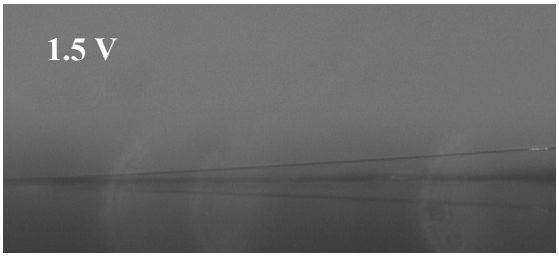
1.5 V


2.0 V


2.5 V


3.0 V

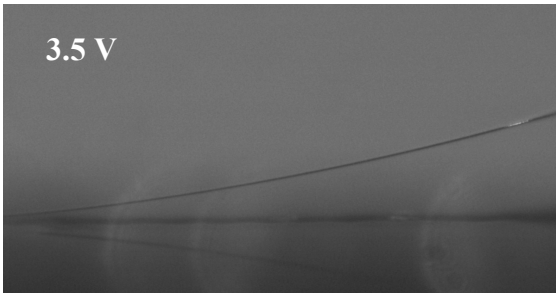
3.5 V

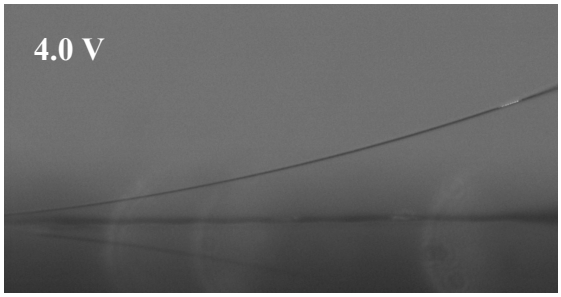
4.0 V

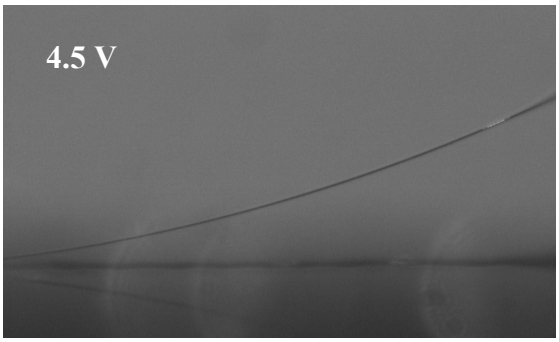
4.5 V

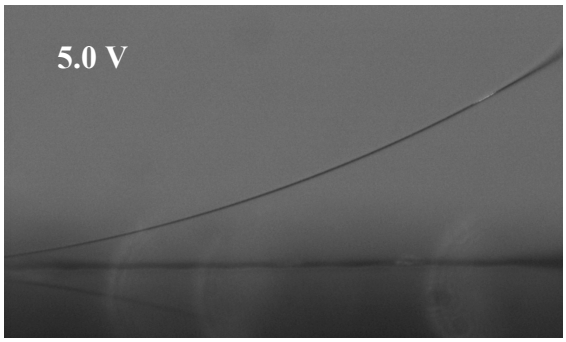
5.0 V

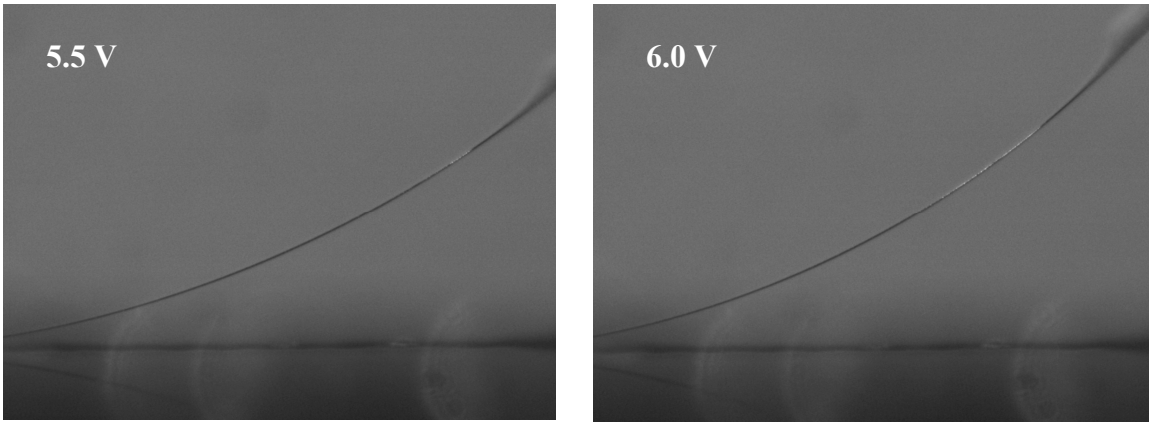

Figure 3.8. PZT beam deflection at different bias voltages 0-6 V.

Similarly, the intersection of the hysteresis loops shifted from negative to positive electric field values at stresses larger than 200 MPa. This intersection point compares the relative population of domains that can remain polarized in one direction vs. the opposite direction upon removal of the electric field. Accounting for the residual stress in the particular PZT layer (112 MPa), this shift occurred at an effective stress of ~310 MPa in the PZT layer. It is also noteworthy that the stress at which the hysteresis loops became symmetric and beyond which the intersection point of the hysteresis loops also remained unchanged was similar to the stress at which the PZT's mechanical behavior became non-linear. This further supports our argument in Chapter 2 that domain switching is responsible for the nonlinear behavior of the PZT material above 0.35% strain (~300 MPa).

The remnant polarization exhibited by a piezoelectric crystal is caused mainly due to 90° switching of domains that are in a metastable state [63]. Higher applied stresses impose greater mechanical constraint on domains that could undergo 90° switching thereby lowering the number of domains that causes hysteresis at ~200 MPa when the remnant polarization is identical on both sides of hysteresis loop. This is due to the presence of equal number of domains able to remain polarized in each direction and may vary for PZT films depending on film thickness, residual stresses and fabrication conditions.

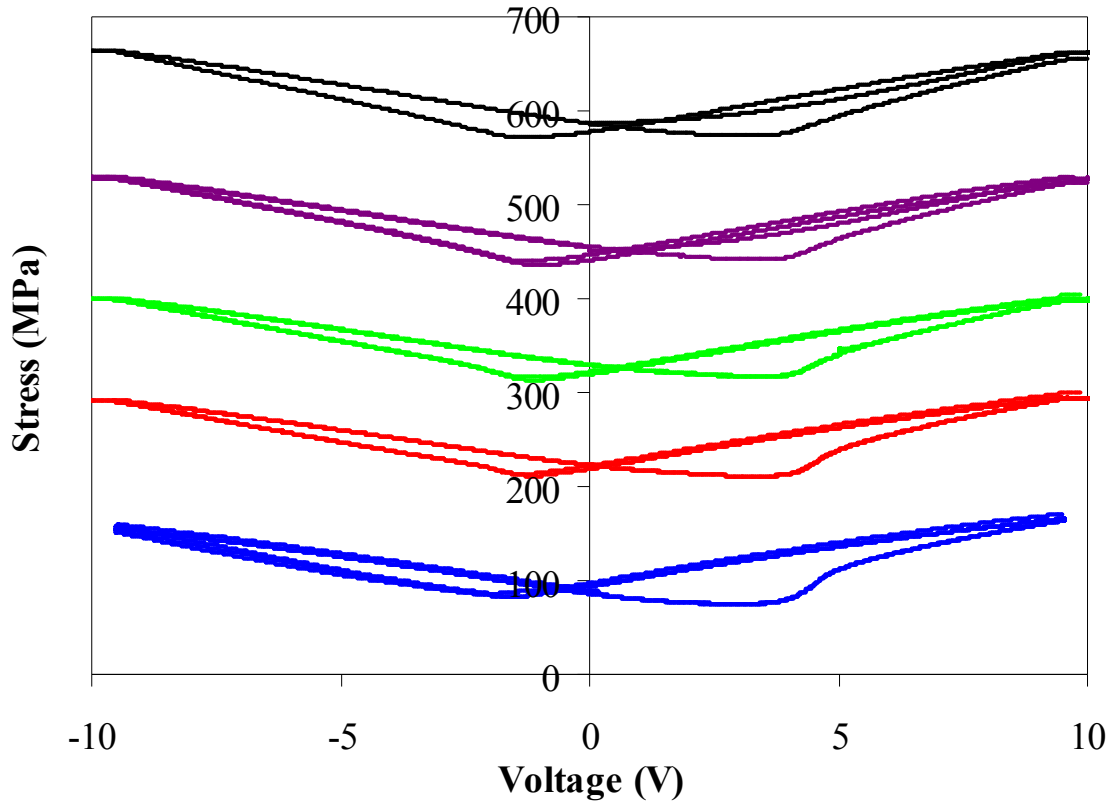

Figure 3.9 Electric field induced stress hysteresis loop for a PZT stack.

The electric field induced lateral strain was calculated for specimens with different preloads. The lateral induced strain calculated via DIC is plotted in Figure 3.10 with respect to the applied bias voltage. The butterfly loops were highly asymmetric possibly due to the unequal population of domains undergoing switching on either direction. Furthermore, due to the clamped-clamped condition of the specimen, it was subjected to an additional stress during application of bias voltage. Hence, the measured strain was a due to the combination of mechanical preload and piezoelectric force generated in the specimen.

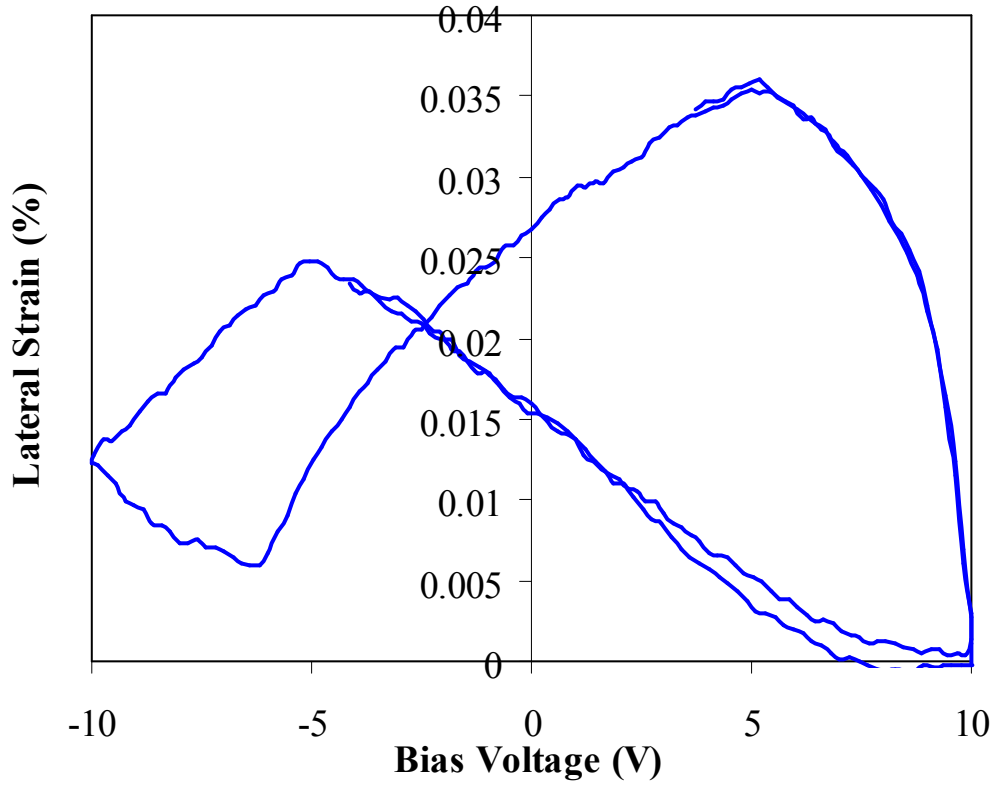

Figure 3.10 Electric field induced lateral strain hysteresis loops at 300 MPa preload.

3.4 Conclusions

In this Chapter, the piezoelectric behavior of sol-gel prepared thin film PZT composites comprised of SiO_2, Pt, PZT and Pt layers was studied to obtain an estimate for the piezoelectric coefficient d_{31} and the response of the film to an applied electric field. The piezoelectric coefficient d_{31} was measured using the multilayered beam bending technique as 385±45 pm/V. At lower applied stresses, the electric field induced stress hysteresis butterfly loops were asymmetric, becoming even at higher applied stresses. The higher applied stresses increased the mechanical constraint on piezoelectric domains preventing them from undergoing 90° switching. This event led to a reduction in the relative population of domains that caused hysteresis. Hence, a decrease in the

magnitude of hysteresis was observed with an increase in the applied stress. Similarly, upon loading, there was a change in the relative number of domains that mainly contributed to one side of the hysteresis loop and therefore, the intersection of the hysteresis loops shifted from a negative to a positive electric field at stresses of about 300 MPa, after accounting for the residual stresses in PZT. This may be directly related to the nonlinear mechanical behavior observed for the PZT films beyond 0.35% strain (~300 MPa) in Chapter 2, owed to significant domain switching after this magnitude of strain.

CHAPTER 4

CONCLUSIONS

The mechanical and piezoelectric behavior of PZT films were investigated according to the objectives stated in Chapter 1. A uniaxial tension testing method for full-field strain measurements was employed to obtain the mechanical properties of thin films made by different combinations of SiO_2, Pt, PZT. The properties measured using our experimental method were very repeatable. This repeatability hinged upon the use of a fine speckle pattern on the specimen surface to resolve small strains. The apparatus built to create the very fine speckle pattern enabled the measurement of displacements with resolution of at least 23 nm. The freestanding SiO_2 thin film specimens tested demonstrated very linear mechanical response with modulus 72.3±2 GPa, failure stress of 1,060±200 MPa and failure strain of 1.4±0.2%. The modulus compared very well with the modulus of 73 GPa for bulk SiO_2. However the high failure strain was attributed to the few defects present in our specimens. With the aid of the fine and dense speckle pattern on the specimen surface, the Poisson's ratio was also calculated as 0.2 for the freestanding SiO_2 thin films, which is reported for the first time for thin film SiO_2 samples. The stress vs. strain curves of SiO_2-TiPt thin films were linear providing a modulus value of 87.9±1 GPa and failure strains of 0.8%, without showing signs of plastic deformation after the 0.6% yield strain of Pt, which was recorded from experiments with single Pt films. The plastic deformation of Pt was delayed by the thick SiO_2 layer in the composite thereby preventing the plastic deformation of Pt. However, at strains higher than 0.8%, the local deformation of Pt triggered failure in the Pt-SiO_2 composites.

On the other hand, the stress vs. strain curves of the PZT composites were nonlinear due to domain switching at strains larger than 0.35%. The initial modulus of PZT at up to 0.3% strain was extracted from the stress vs. strain curves of SiO_2, SiO_2-TiPt, SiO_2-TiPt-PZT, and SiO_2-TiPt-PZT-Pt freestanding films, by using simple laminate theory, as 84±2 GPa with the failure strength averaging 510±35 MPa, after accounting for the residual stress in the PZT layer.

Finally, PZT stacks with similar dimensions, fabricated in the same lot, were employed to measure the piezoelectric coefficient d_{31} and their hysteretic response. The multilayer beam bending technique was used to measure the d_{31} coefficient as 385±45 pm/V. The alternating electric field induced stress hysteresis "butterfly" loops that were asymmetric at smaller applied stresses, becoming symmetric at higher applied stresses which corresponded to the stress at which the PZT films showed elastic softening. Due to a change in the number of domains that switched with the applied stress, the intersection of the hysteresis loops shifted from the negative to positive electric field at about 200 MPa of applied pre-stress. This non-linear electromechanical behavior can have significant effect on the performance of MEMS devices when operated at higher loads due to the inaccurate estimate of stress and strain associated the application of a combination of a voltage bias and a mechanical stress.

The mechanical and piezoelectric properties measured in this dissertation can be the basis for design and fabrication of PZT based MEMS devices for sensing and actuation purposes. This research serves as a solid ground work for future research to investigate the effect of PZT film thickness, poling and grain structure on the piezoelectric response of sol-gel prepared PZT thin films.

Appendix A

Matlab code for calculating d_{31} piezoelectric coefficient

```
h=[1.050E-07, 0.94E-06, 1.89E-07, 5.15E-07];
w=[1.00E-04, 1.00E-04, 1.00E-04, 1.00E-04];
E=[1.73E+11, 8.40E+10, 1.73E+11, 7.23E+10];
S=[5.78035E-12, 1.19048E-11, 5.78035E-12, 1.38313E-11];
d31=[0,415e-12,0,0];
x=1e-3;
U=6;

ztemp1=0;
for i=1:4

   ztemp1=w(i)*h(i)*h(i)/S(i)+ztemp1;
 end

ztemp1;

ztemp2=0;

for i=1:4
   su=0;
   for j=1:i
      su=su+h(j);
   end
   ztemp2=w(i)*h(i)/S(i)*su + ztemp2;
end
ztemp2;
ztemp3=0;

for i=1:4
   ztemp3=w(i)*h(i)/S(i)+ztemp3;
end
```

```
ztemp3;

z=-(ztemp1-2*ztemp2)/2/ztemp3

ctemp1=0;
for i=1:4
   su1=0;
   su2=0;

   for j=1:i
   su1=su1+h(j);
   end

   for k=1:i-1
      su2=su2+h(k);
   end

      ctemp1=w(i)/S(i)*(3*h(i)*(z-su1)*(z-su2)+h(i)^3) + ctemp1;
end

c=1/3*ctemp1;

mpiezo=0;
for i=1:4

   su1=0;
   for j=1:i
   su1=su1+h(j);
   end

   mpiezo=w(i)*d31(i)/S(i)/h(i)*(2*z*h(i)-2*h(i)*su1+h(i)^2)+mpiezo;
end
mpiezo=mpiezo/2;
deflection=U*mpiezo/2/c*x*x
curvature = U*mpiezo/c
radius=1/curvature
```

REFERENCES

[1] J. Zhou, S. Dasgupta, H. Kobayashi, J.M. Wolff, H.E. Jackson, and J.T. Boyd, "Optically interrogated MEMS pressure sensors for propulsion applications", *Optical Engineering*, 40, pp. 598-604, 2001

[2] S. Kamisuki, M. Fujii, T. Takekoshi, C. Tezuka, M. Atobe, "A high resolution, electrostatically-driven commercial inkjet head*," Proceedings of the IEEE Micro Electro Mechanical Systems (MEMS)*, pp.793-798, 2000

[3] V.K. Varadan, V.V. Varadan, "Microsensors, microelectromechanical systems (MEMS), and electronics for smart structures and systems", *Smart Materials and Structures*, 9, pp.953–972, 2000

[4] M. Douglass, "DMD reliability: A MEMS success story" *Proceedings of SPIE - The International Society for Optical Engineering*, 4980, pp.1, 2003

[5] C. Liao, J. Tsai, "The Evolution of MEMS Displays", *IEEE Transactions on Industrial Electronics,* 56, pp. 1057-1065, 2009

[6] J. Kimberley, R.S. Cooney, J. Lambros, I. Chasiotis, N.S. Barker, "Failure of Au RF-MEMS switches subjected to dynamic loading", *Sensors and Actuators A: Physical*, 154 (1), pp. 140-148,2009.

[7] http://mems.sandia.gov/gallery/images/tg8.jpg

[8] http://www.chipworks.com

[9] R. Polcawich, D. Judy, J. Pulskamp, S. Trolier-McKinstry, M.Dubey, "Advances in Piezoelectrically Actuated RF MEMS Switches and Phase Shifters", *Microwave Symposium IEEE/MTT-S International*, pp. 2083-2086, 2007

[10] Hsien-Chun Chung, K. Lal Kummari, S.J. Croucher, N.J. Lawson, S. Guo, R.W. Whatmore, Z. Huang, "Development of piezoelectric fans for flapping wing application", *Sensors and Actuators A: Physical*, 149 (1), pp. 136-142, 2009.

[11] Y.H Aiguo Ming, Y. Fukushima, M. Shimojo, "Development of an active flapping wing using Piezoelectric Fiber Composites", *Proceedings of the 2008*

IEEE, International Conference on Robotics and Biomimetics, pp. 2144-2149, 2009

[12] D. Judy, J. Pulskamp, R. Polcawich, L. Currano, "Piezoelectric Nanoswitch", *IEEE 22nd International Conference on Micro Electro Mechanical Systems*, pp.591-594, 2009

[13] W. Choi, Y. Jeon, J. Jeong, R. Sood, S. Kim, " Energy harvesting MEMS device based on thin film piezoelectric cantilevers", *Journal of Electroceramics*, 17, pp. 543-548, 2006

[14] S. Kim, W. Clark, Q. Wang, "Piezoelectric Energy Harvesting with a Clamped Circular Plate: Experimental Study", *Journal of Intelligent Material Systems and Structures*, 16 (10), pp. 855-863, 2005

[15] S. Priya, "Advances in energy harvesting using low profile piezoelectric transducers", *Journal of Electroceramics*, 19 (1), pp. 167-184, 2007

[16] M. Ramsay, W. Clark, "Piezoelectric energy harvesting for bio MEMS applications", *Proceedings of SPIE - The International Society for Optical Engineering*, 4332, pp. 429-438, 2001

[17] W. Choi,Y. Jeon, J. Jeong, R. Sood, S. Kim, "Energy harvesting MEMS device based on thin film piezoelectric cantilevers", *Journal of Electroceramics*, 17 (2-4), pp. 543-548, 2006

[18] Y. Jeona, R. Soodb, J. Jeongc, S. Kimd, "MEMS power generator with transverse mode thin film PZT", *Sensors and Actuators A: Physical*, 122 (1), pp. 16-22, 2005

[19] E. Kruglick, K. Pister, "Lateral MEMS microcontact considerations" *Journal of Microelectromechanical Systems,* 8 (3), pp. 264-271, 1999

[20] W. Huang, G. Lu, "Analysis of lateral instability of in-plane comb drive MEMS actuators based on a two-dimensional model", *Sensors and Actuators A: Physical,* 113 (1), pp. 78-85, 2004

[21] B. Borovic, F. Lewis, A. Liu, E. Kolesar, D. Popa, "The lateral instability problem in electrostatic comb drive actuators: Modeling and feedback control", *Journal of Micromechanics and Microengineering*, 16 (7), pp. 1233-1241, 2006

[22] M. Naraghi, I. Chasiotis, "Optimization of Comb-driven Devices for Mechanical Testing of Polymeric Nanofibers Subjected to Large Deformations" *Journal of Microelectromechanical Systems* 18 (5), pp. 1032-1046, 2009

[23] R. Emery, G. Povirk, "Tensile behavior of free-standing gold films. Part I. Coarse-grained films", *Acta Materialia*, 51 (7), pp. 2067-2078, 2003

[24] R. Emery, G. Povirk, "Tensile behavior of free-standing gold films. Part II. Fine-grained films", *Acta Materialia*, 51 (7), pp. 2067-2078, 2003

[25] B. Boyce, M. Shawa, P. Lua, M. Duggera "Stronger silicon for microsystems", *Acta Materialia* (article in press)

[26] A. Mathur, J. Erlebacher, "Size dependence of effective Young's modulus of nanoporous gold", *Applied Physics Letters*, 90 (6), art. no. 061910, 2007

[27] D. Faurie, P. Renault, E. Le Bourhis, Ph. Goudeau, "Study of texture effect on elastic properties of Au thin films by X-ray diffraction and in situ tensile testing", *Acta Materialia*, 54 (17), pp. 4503-4513, 2006

[28] H. Espinosa, B. Prorok, "Size effects on the mechanical behavior of gold thin films", *Journal of Materials Science*, 38 (20), pp. 4125-4128, 2003

[29] N. Karanjgaokar, K. Jonnalagadda, I. Chasiotis, J. Chee, A. Mahmood, D. Peroulis, "Mechanical behavior of nanocrystalline Au films as a function of strain rate and film thickness", *Society for Experimental Mechanics - 11th International Congress and Exhibition on Experimental and Applied Mechanics*, 4, pp. 1860-1866, 2008

[30] I. Chasiotis, C. Bateson, K. Timpano, A. McCarty, N. Barker, J. Stanec, "Strain rate effects on the mechanical behavior of nanocrystalline Au films", *Thin Solid Films*, 515 (6), pp. 3183-3189, 2007.

[31] L. Wang, B. Prorok, "Characterization of the strain rate dependent behavior of nanocrystalline gold films", *Journal of Materials Research*, 23 (1), pp. 55-65, 2008

[32] I. Chasiotis, W. Knauss, "The mechanical strength of polysilicon films: Part 1. The influence of fabrication governed surface conditions", *Journal of the Mechanics and Physics of Solids*, 51 (8), pp. 1533-1550, 2003

[33] D. Bhar, J. Robach, J. Wright, L. Francis, W. Gerberich, "Mechanical deformation of PZT thin films for MEMS applications", *Materials science and Engineering*, 259, pp. 126-131, 1999

[34] T. Fang, S. Jian, D. Chuu, "Nanomechanical properties of lead zirconate titanate thin films by nanoindentation", *Journal of Physics: Condensed Matter*, 15, pp. 5253-5259, 2003

[35] J. Zhou, T. McMcollough, S. Mantell, S. Zurn, "Young's Modulus Measurement of Thin Film PZT", *Proceedings of 13 biennial Microelectronics symposium*, pp. 153-157, 1999

[36] S. Hong, M. Kim, S. Lee, C.S. Lee, "Characterization of Deformation Behaviors and Elastic Moduli of Multilayered Films in Piezoelectric Inkjet Head", *Journal of Microelectro Mechanical Systems*, 17 (5), pp. 1155-1163, 2008

[37] S. Wakabayashi, H. Totani, M.Sakata, M. Ikeda, H. Goto, M. Takeuchi, T.Yada, "Study on mechanical characteristics of PZT thin film for sensors and actuators", *Proceedings of SPIE - The International Society for Optical Engineering*, 2639, pp. 304-314, 1995

[38] T. Ohmi, K. Kotani, A. Teramoto, M. Miyashita,"Dependence of electron channel mobility on Si-SiO2 interface microroughness", *Electron device letters*, 12 (12), pp. 652-654, 1995

[39] C. Yeh, S.S. Lin, T. Yang, C. Chen, Chun-Lin, Y.Yang, "Performance and off-state current mechanisms of low-temperature processed polysilicon thin-film

transistors with liquid phase deposited SiO2 gate insulator", *IEEE Transactions on Electron Devices,* 41, (2), pp. 173-179, 1994

[40] A. Morales, A. Duran,"Sol-Gel Protection of Front Surface Silver and Aluminum Mirrors", *Journal of Sol-Gel Science and Technology*, 8 (1-3), pp. 451-457, 1997

[41] C. Ballif, J. Dicker, D. Borchert, T. Hofmann, "Solar glass with industrial porous SiO2 antireflection coating: measurements of photovoltaic module properties improvement and modelling of yearly energy yield gain", *Solar Energy Materials and Solar Cells*, 82 (3), pp. 331-344, 2004

[42] F. Helvaci, J. Cho, "A Nanoindentation Study of Thermally-Grown-Oxide Films on Silicon", *Materials Research Society*, 841, pp. 375-380, 2005

[43] J. Yang, O. Paul, "Fracture Properties of Thermal Silicon Oxide Thin Films from the Load-Deflection of Long SiN_X/SiO_2", *Proceedings of 1st IEEE International Conference on Nano/Micro Engineered and Molecular Systems,* pp. 1362-1367, 2006

[44] Y. Su, C. Qian, M. Zhao, T. Zhang, "Microbridge Testing of Silicon Oxide /Silicon Nitride Layer Films Deposited on Silicon Wafers", *Acta Materialia*, 48, pp. 4901-4915, 2000

[45] W. Sharpe, J. Pulskamp, D. Gianola, C. Eberl, R. Polcawich, J. Thompson, "Strain Measurements of Silicon Dioxide Microspecimens by Digital Imaging Processing", *Experimental Mechanics*, 47, pp. 649-658, 2007

[46] M. Lin, P. Deiry, R. Chromik, N. Barbosa, W. Brown, T. Delph, R. Vinci, "Temperature-dependent microtensile testing of thin film materials for application to microelectromechanical system", *Microsystem Technologies*, 12, pp. 1045-1051, 2006

[47] K. Jonnalagadda, I. Chasiotis, S. Yagnamurthy, J. Lambros, J. Pulskamp, R. Polcawich, M. Dubey, "Experimental Investigation of Strain Rate Dependence of Nanocrystalline Pt Films", *Experimental Mechanics*, Published online 2009. doi: 10.1007/s11340-009-9259-0

[48] K. Budd, S. Dey, and D. Payne, “Sol-gel processing of PbTiO3, PbZrO3, PZT, and PLZT thin films,” *Proceedings of Brittle Ceramics*, 36, pp. 107-121, 1985

[49] I. Chasiotis, W. Knauss, “A New Microtensile Tester for the Study of MEMS Materials with the aid of Atomic Force Microscopy”, *Experimental Mechanics,* 42 (1), pp. 51-57, 2002

[50] S. Cho, I. Chasiotis, “Elastic Properties and Representative Volume Element of Polycrystalline Silicon for MEMS,” *Experimental Mechanics*, 47 (1), pp. 37-49, 2007

[51] M. Naraghi, I. Chasiotis, Y. Dzenis, Y. Wen, H. Kahn, “Novel Method for Mechanical Characterization of Polymeric Nanofibers”, *Review of Scientific Instruments*, 78, art. no. 085108, 2007

[52] J. Fan, W. Stoll, C. Lynch, "Nonlinear constitutive behavior of soft and hard PZT: Experiments and modeling", *Acta Materialia*, 47 (17), pp. 4415-4425, 1999

[53] F. Xu, S. Trolier-McKinstry, W. Ren, B. Xu, Z. Xie, K. Hemker, "Domain wall motion and its contribution to the dielectric and piezoelectric properties of lead zirconate titanate films", *Journal of Applied Physics*, 89 (2), pp. 1336-1348, 2001

[54] H. Cao, A. Evans, "Nonlinear Deformation of Ferroelectric Ceramics" *Journal of the American Ceramic Society*, 76 (4), pp. 890-896, 1993

[55] T. Tanimoto, K. Yamamoto, T. Morii, "Nonlinear Stress-Strain Behavior of Piezoelectric Ceramics under Tensile Loading", *Proceedings of the Ninth IEEE International Symposium on Applications of Ferroelectrics*, pp. 394-397, 1994

[56] S.P. Beeby, N.J. Grabham, N.M. White, "Microprocessor implemented self-validation of thick-film PZT/silicon accelerometer", *Sensors and Actuators A: Physical*, 92 (1-3), pp. 168-174, 2001

[57] R. Polcawich, M. Scanlon, J. Pulskamp, J. Clarkson, J. Conrad, D. Washington, R. Piekarz, S. Trolier, M.Dubey, "Design and fabrication of a lead zirconate titanate (PZT) thin film acoustic sensor", *Integrated Ferroelectrics*, 54 (1), pp. 595-606, 2003

[58] C. Fox, X. Chen, H.W. Jiang, P.B. Kirby, S. McWilliam, "Development of micromachined RF switches with piezofilm actuation", *Proceedings of SPIE - The International Society for Optical Engineering*, 4700, pp. 40-49, 2002

[59] Y. Nemirovsky, A. Nemirovsky, P. Muralt, N. Setter, "Design of a novel thin-film piezoelectric accelerometer" *Sensors and Actuators A: Physical*, 56 (3), pp. 239-249, 1996

[60] K. Maenaka, H. Kohara, M. Nishimura, T. Fujita, Y. Takayama, "Novel solid micro-gyroscope", *Proceedings of the IEEE International Conference on Micro Electro Mechanical Systems (MEMS)*, 1627879, pp. 634-637, 2006

[61] B. Piekarski, M. Dubey, E. Zakar, R. Polcawich, D. DeVoe, D. Wickenden, "Sol-Gel PZT for MEMS Applications" *Integrated Ferroelectrics*, 42, pp. 25-37, 2002

[62] S. Trolier-McKinstry, P. Muralt, "Thin Film Piezoelectrics for MEMS", *Journal of Electroceramics*, 12(1-2), pp. 7-17, 2004

[63] B. Jaffe, W.R. Cook, H. Jaffe, "Piezoelectric Ceramics", *Academic Press London and Newyork*, 1971

[64] H.J. Hwang, T. Nagai, T. Ohji, M. Sando, M. Toriyama, K. Niihara, "Curie Temperature Anomaly in Lead Zirconate Titanate/Silver Composites" *Journal of the American Ceramic Society*, 81 (3), pp. 709-712, 2005

[65] J. Cheng, N. Li, L.E. Cross, Z. Meng, "Self-poling Effects in Sol-gel Derived Pb(Zr1-xTix)O3 Thin Films", *Materials Research Society Symposium – Proceedings,* 748, pp. 179-185, 2003

[66] http://www.physikinstrumente.com

[67] The world of Micro- and Nanopositioning, *Physikinstrumente products manual*, 2005-06

[68] Z. Surowiak, M.F. Kupriyanov, D. Czekaj, "Properties of nanocrystalline ferroelectric PZT ceramics", *Journal of the European Ceramic Society*, 21, pp. 1377–1381, (2001)

[69] H.Z. Jin, J. Zhu, "Size effect and fatigue mechanism in ferroelectric thin films", *Journal of Applied Physics*, 92, pp. 4594–4598, (2002)

[70] S. Buhlmann, B. Dwir, J. Baborowski, P. Muralt, "Size effect in mesoscopic epitaxial ferroelectric structures: increase of piezoelectric response with decreasing feature size", *Applied Physics Letters*, 80, pp. 3195–3197, (2002)

[71] S. Yokoyama, T. Ozeki, T. Oikawa, H. Funakubo, "Preparation of orientation-controlled polycrystalline Pb(Zr,Ti)O3 thick films on (1 0 0) Si substrates by metalorganic chemical vapor deposition and their electrical properties", *Japanese Journal of Applied Physics*, 41, pp. 6705–6708, (2002)

[72] M.C. Kim, J.W. Choi, S.J. Yoon, K.H. Yoon, H.J. Kim, "Thickness dependence of Pb(Zr0.52Ti0.48)O3 films prepared by pulsed laser deposition", *Japanese Journal of Applied Physics*, 41, pp. 3817–3821, (2002)

[73] Y.L. Tu, M.L. Calzada, N.J. Phillips, S.J. Milne, "Synthesis and electrical characterization of thin films of PT and PZT made from a diol-based sol–gel route", *Journal of American Ceramics Society*, 79, pp. 441–448, (1996)

[74] S. Trolier-McKinstry, J.F. Shepard Jr., J.L. Lacey, T. Su, G. Zavala, J. Fendler, "Piezoelectricity in ferroelectric thin films: Domain and stress issues", *Ferroelectrics*, 206-207 (1 -4; 1-2), pp. 381-392, 1998

[75] R.A. Dorey, R.W. Whatmore, "Apparent reduction in the value of the d(33) piezoelectric coefficient in PZT thick films", *Integrated Ferroelectrics*, 50, pp.111-119, 2002

[76] C.D.E. Lakeman, D.A. Payne, "Apparent thickness effect on properties of ferroelectric PZT thin layers", *Ferroelectrics*, 152, pp. 145–150, (1994)

[77] Z. Surowiak, M.F. Kupriyanov, D. Czekaj, "Properties of nanocrystalline ferroelectric PZT ceramics", *Journal of the European Ceramic Society*, 21, pp. 1377–1381, (2001)

[78] H.Z. Jin, J. Zhu, "Size effect and fatigue mechanism in ferroelectric thin films", *Journal of Applied Physics*, 92, pp. 4594–4598, (2002)

[79] X.H. Du, J. Zheng, U. Belegundu, K. Uchino, "Crystal orientation dependence of piezoelectric properties of lead zirconate titanate near the morphotropic phase boundary", *Applied Physics Letters*, 72, pp. 2421–2423, (1998)

[80] S. Trolier-Mckinstry, P. Muralt, "Thin film piezoelectrics for MEMS", *Journal of Electroceramics*, 12, (1-2), pp. 7-17, 2004

[81] C. Ayela, L. Nicu, C. Sover, E. Cattan, C. Bergaud, "Determination of the d31 piezoelectric coefficient of PbZrxTi1-xO3 thin films using multilayer buckled micromembranes", *Journal of applied physics*, 100, 054908, 2006

[82] K. Lefki, G.J.M. Dormans, "Measurement of piezoelectric coefficients of ferroelectric thin films", *Journal of Applied Physics*, 76, pp. 1764-1767, 1994

[83] N. Tagawa, H. Seki, K. Kitamura, A. Mori, "Development of novel PZT thin films for active sliders based on head load/unload on demand systems", *Microsystem Technologies*, 8 (2-3), pp. 133-138, 2002

[84] T. Kobayashi, J. Tsaur, M. Ichiki, R. Maeda, "Fabrication and performance of a flat piezoelectric cantilever obtained using a sol–gel derived PZT thick film deposited on a SOI wafer", *Smart Materials and Structures*, 15 (1), pp. S137-S140, 2006

[85] J. Akedo, M. Lebedev, "Piezoelectric properties and poling effect of Pb(Zr, Ti)O3 thick films prepared for microactuators by aerosol deposition", *Applied Physics Letters*, 77 (11), pp. 1710-1712, 2000

[86] Z. Zhao, Z. Luo, C. Liu, W. Wu, C. Gao, Y. Lu, "Quantitative measurement of piezoelectric coefficient of thin film using a scanning evanescent microwave microscope", *Review of Scientific Instruments*, 79 (6), 064704, 2008

[87] R.J. Ong, T.A. Berfield, N.R. Sottos, D.A Payne, "Sol-Gel derived Pb(Zr,Ti)O3 thin films: Residual stress and electrical properties", *Journal of the European Ceramic Society*, 25, pp. 2247-2251, 2005

[88] T.A. Berfield, R.J. Ong, D.A. Payne, N.R Sottos, "Residual stress effects on piezoelectric response of sol-gel derived lead zirconate titanate thin films", *Journal of Applied Physics*, 101 (2), 024102, 2007

[89] J.M. Liu, B. Pan, H. Chan, S.N. Zhu, Y.Y Zhu, Z.G. Liu, "Piezoelectric coefficient measurement of piezoelectric thin films: An overview ", *Materials Chemistry and Physics*, 75 (1-3), pp. 12-18, 2002

[90] R. Ballas, H. Schlaak, A. Schmid, "The constituent equations of piezoelectric multilayer bending actuators in closed analytical form and experimental results", *Sensors and Actuators, A: Physica*,l 130-131, pp. 91-98.2006

[91] T.A. Berfield, "Residual stress development and effect on the piezoelectric performance of sol-gel derived Lead Zirconate Titanate (PZT) thin films", *PhD dissertation*, 2008